Robotics and Computer-Integrated Manufacturing 44 (2017) 156–173

Contents lists available at ScienceDirect

Robotics and Computer-Integrated Manufacturing

journal homepage: www.elsevier.com/locate/rcim

Adaptive positioning control of an ultrasonic linear motor system

Jia-Si Mo, Zhi-Cheng Qiu, Jun-Yang Wei, Xian-Min Zhang *

Guangdong Province Key Laboratory of Precision and Manufacturing Technology, South China University of Technology, Guangzhou 510641, China

ARTICLE INFO

Article history:
Received 9 September 2015
Received in revised form
10 August 2016
Accepted 10 August 2016
Available online 29 August 2016

Keywords:
Ultrasonic linear motor
Friction compensation
Dead-zone
Adaptive positioning control

ABSTRACT

A 3PRR parallel precision positioning system, driven by three ultrasonic linear motors, was designed for use as the object stage of a scanning electron microscope (SEM). To improve the tracking accuracy of the parallel platform, the positioning control algorithms for the drive joints needed to be studied. The dead-zone phenomenon caused by static friction reduces the trajectory tracking accuracy significantly. Linear control algorithms such as PID (Proportion Integration Differentiation) are unable to compensate effectively for the dead-zone nonlinearity. To address this problem, two types of feedforward compensation control algorithms have been investigated. One is constant feedforward with the integral separation PID; the other is adaptive feedback and feedforward based on the model reference adaptive control (MRAC). Simulations and experiments were conducted using these two control algorithms. The results demonstrated that the constant feedforward with integral separation PID algorithm can compensate for the time-invariant system after identifying the dead-zone depth, while the adaptive feedback and feedforward algorithm is more suitable for the time-varying system. The experimental results show good agreement with the simulation results for these two control algorithms. For the dead-zone nonlinearity caused by the static friction, the adaptive feedback and feedforward algorithm can effectively improve the trajectory tracking accuracy.

1. Introduction

The micro-nano operating system is an important part in the field of precision operation. Such systems are usually comprised of compliant mechanisms and can fulfill the requirements of high-precision positioning but are unable to perform large-scale positioning [1]. The object stage of the micro-nano operating system is used to carry the samples for large-scale motions. Therefore, the object stage must meet the requirements of both large-stroke and high-precision positioning. A parallel mechanism usually accompanies the precision positioning system, so a 3PRR parallel precision positioning system driven by an ultrasonic linear motor has been designed and used as the object stage of a scanning electron microscope (SEM). The accuracy of the drive joints affects the accuracy of the end-effector. There are some nonlinearities, such as the friction, elastic deformation and backlash clearance, that will affect the joint positioning accuracy, or give rise to problems such as stick slip, limit cycle [2] and steady-state error [3], even leading to a bad working situation of self-excited vibration [4]. To the effect of the nonlinearities, there are two valid methods: one is to introduce less nonlinearity in the design process, while the other is to apply a nonlinear control algorithm to compensate for the nonlinearity [5]. Adaptive control is usually applied for the nonlinear control [6–8].

The ultrasonic linear motor is free of backlash clearance, and the clearance of the linear slider can be eliminated by preloading. Thus, the ultrasonic linear motor positioning system has no backlash clearance and less elastic deformation, and the main nonlinearity is the friction. Friction is always the main obstacle for high-precision positioning. Castillo-Castaneda has shown that friction influences accuracy much more than clearance [5]. Moreover, the static friction is the main factor affecting the trajectory tracking accuracy, leading to time delay and a dead-zone [9]. Friction compensation has been widely used for precision positioning. The friction model is a research hotspot and is not mature. There is as yet no perfect model to describe various friction behaviors [10]. The static friction behaviors are complex at the micro level and significantly affect the positioning accuracy [11–14]. The ultrasonic linear motor used in this 3PRR positioning system is a stick-slip type motor, and the two drive feet rub the rod at an ultrasonic frequency, allowing the motor to move forward. This design is different from other ultrasonic linear motors. The ultrasonic linear motor used in references [15–17] is the resonant vibration type motor, and the trajectory of the spacer is an ellipse. Different types of motor have different driving characteristics. The friction acts as a drive source and a resistance source at the same time, especially at low speed. The motor exhibits a strong nonlinearity that must be compensated. The neural network is an

* Corresponding author.
E-mail address: zhangxm@scut.edu.cn (X.-M. Zhang).

http://dx.doi.org/10.1016/j.rcim.2016.08.011

effective method for nonlinear control. References [15–17] control the ultrasonic linear motor using a neural network with good control performance, which is very enlightening regarding ultrasonic linear motor control. It can compensate for a part of the flat peak phenomenon but cannot eliminate it thoroughly.

Friction compensation can be divided into two types. One is based on a friction model; the other is a model-free method. The first step of the model-based compensation method is to build a suitable model of the friction, from a mathematical perspective. It is difficult to obtain a perfect model of the friction force. Many scholars have researched friction extensively and proposed many types of models, successively including the Coulomb model, the Stribeck model [18], the Dahl model [19], the LuGre model [10], the Leuven model [20] and so on. Because the LuGre model includes multiple types of friction behaviors such as Coulomb friction, pre-sliding friction, and friction lag, it is widely used in friction compensation [21,22]. Although the LuGre model is useful in friction compensation, it is not convenient for the friction compensation of an ultrasonic linear motor. Some of the model parameters cannot be identified, and it is difficult to express the friction behaviors under ultrasonic vibration. The static friction can be modeled as a dead-zone nonlinearity [9,14], so dead-zone compensation methods are also useful for static friction compensation [23–26]. The literature [27] has compared several control algorithms for the tracking control of an ultrasonic linear motor actuated stage; combinations with feedforward control exhibit better control performance.

This study aims to solve the flat peak phenomenon when the system is tracking a sine wave trajectory. The flat peak phenomenon is caused by static friction and is difficult to compensate for via feedback control alone [5,28], so feedforward control is introduced to improve the tracking accuracy. Aiming at cases of unknown friction models, the model-free method for friction compensation was developed. This method is designed for this motor type and treats the friction nonlinearity as the disturbance, compensating for it in real time. Two feedforward control algorithms are utilized: one is constant feedforward combined with PID control, while the other is adaptive feedforward combined with the MRAC. Constant value compensation with the integral separation PID control is studied. It is a modified PID control method that can compensate for the time delay and the flat peak of the sine wave trajectory tracking. This method can improve the trajectory tracking accuracy of the system. However, it cannot adjust the compensation parameter adaptively when there is a disturbance or uncertainty in the friction interface. The adaptive feedback and feedforward algorithm is applied to solve this problem. The experimental results demonstrated that both model-free methods can effectively compensate for the friction.

The rest of this article is organized as follows. Section 2 presents the system description and problem statement. Section 3 introduces the constant feedforward with integral separation PID method and describes the simulation. Section 4 introduces the adaptive feedback and feedforward algorithm and describes the simulation. Section 5 presents the experimental results of the control algorithms. Section 6 draws the conclusions and summarizes the proposed work.

2. System description and problem statement

The 3PRR planar parallel mechanism has been designed and built as an object stage for the SEM. The trajectory tracking precision requires improvement, so it is necessary to investigate control methods for the ultrasonic linear motor positioning system. Due to the high response and precise performance of the ultrasonic motor [29], mechanisms driven by ultrasonic linear motor can accomplish the requirements of high speed, high precision and no magnetic field. The static friction in the system decreases the trajectory tracking accuracy, and the phenomenon of static friction has been investigated in subsequent experiments.

2.1. System description

The parallel 3PRR precision positioning system has been designed to meet the demands of precision positioning, shown in Fig. 1(b). It consists of the ultrasonic linear motor positioning system shown in Fig. 1(a). The ultrasonic linear motor positioning system is an electromechanical system including a computer and control card, motor driving unit and motor. The computer is used as the host and calculates the control value through a specified control algorithm. Then, the control value is sent to the control card, which translates it to a voltage signal. The motor driving unit receives the voltage signal and translates it to a high-frequency, high-amplitude driving voltage to the PZT inside the ultrasonic linear motor case. Therefore, the motor moves in a specified velocity carrying the linear encoder, the displacement and the velocity feedback to the control card and the computer, making up closed-loop system.

According to the design method described above, the ultrasonic linear motor positioning system was constructed as an experimental apparatus to verify the control methods for reducing nonlinearities. It is well known that simpler and more reliable mechanisms introduce fewer errors, such as the assembly error and machining error. Furthermore, because the simple mechanism consists of fewer parts, less nonlinearity is introduced. The ultrasonic linear motor driven system is a direct drive system. It does not include a ball screw and gear reducer, and it is driven by preloaded friction, with less backlash clearance. The ultrasonic linear motor positioning system is also free of magnetic fields. Therefore, it is adapted to environments without magnetic fields, such as the SEM chamber, as shown in Fig. 1(c).

The driving principle of the ultrasonic linear motor is shown in Fig. 2. The low-speed high-thrust characteristic makes it suitable for direct drive with no gear reducer transmission mechanism, and the linear type of ultrasonic motor moves straight without connecting to a ball screw, so it has no backlash clearance. The ultrasonic linear motor is a piezoelectric motor powered by the ultrasonic vibration of the stator, placed against the rotor. This system uses the motor model type U-264 made by PI German. The rod of the motor acts as the stator, and the two drive feet in the motor case act as the rotor.

2.2. Problem statement

1) The uncertainty of the friction interface on the motor rod leads to different running states in different travel ranges and different times. The parameters of the friction model are difficult to identify.

The friction model shows that the state of the friction interface, such as roughness and lubrication, can affect the friction parameters [30]. The ultrasonic linear motor is driven by friction. Two PZT units are connected to the driving feet and clamped to the motor rod. When applying the control voltage signal to the motor drive unit, the motor drive excites the feet to rub the rod, causing motion. The drive principle of the motor is shown in Fig. 2. Hence, the friction interface of the motor on the motor rod is the key factor affecting the running state.

The uncertainty of the friction interface includes two aspects: the slow time-varying and the inconsistency of the friction interface. The rod is exposed to the air, so environmental changes such

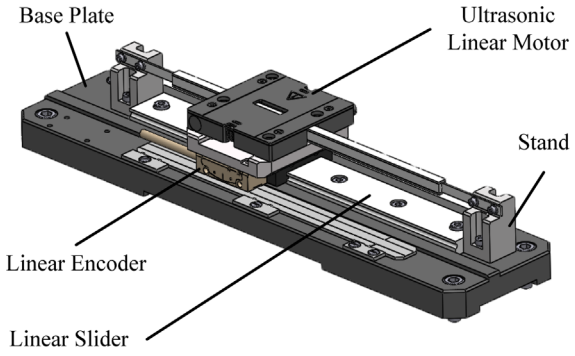

(a) Design of the ultrasonic linear motor positioning system

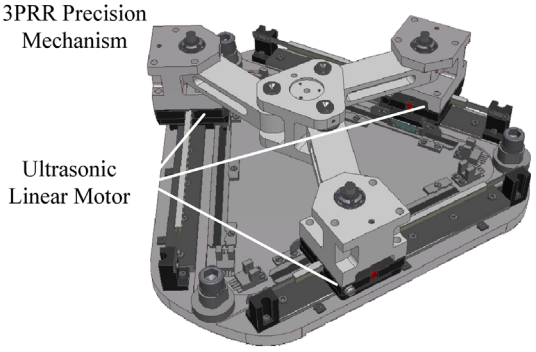

(b) 3PRR mechanism driven by ultrasonic linear motor

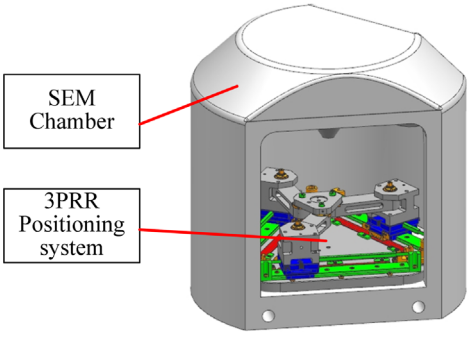

(c) 3PRR object stage in SEM chamber

Fig. 1. 3D diagram of the driving unit and the parallel platform. (a) Design of the ultrasonic linear motor positioning system. (b) 3PRR mechanism driven by ultrasonic linear motor. (c) 3PRR object stage in SEM chamber.

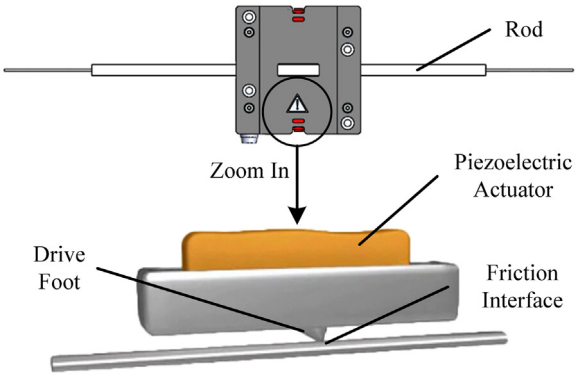

Fig. 2. Driving principle of the ultrasonic linear motor (U-264 from PI German).

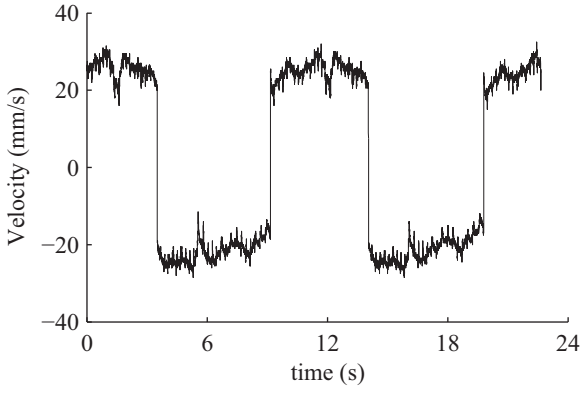

Fig. 3. Velocity curve when applying 1.5 V drive voltage.

as dust and humidity will affect the friction interface of the rod. The ultrasonic linear motor is sensitive to the friction parameter change and behaves as the velocity change when applying the same drive voltage for different time. The rod is too long to ensure the consistency of the friction interface. The inconsistency of the friction interface on the motor rod affects the velocity asymmetrically at the same drive voltage. Fig. 3 shows that the velocity is asymmetrical for the full travel range when applying the drive voltage of 1.5 V, and the results are similar at other drive voltages.

To determine the relationships between the drive voltage and velocity and between the drive voltage and friction, experimental friction identification was performed. By applying a linear voltage to the motor drive and recording the average velocity of the motor, the relationship between the voltage and velocity is obtained, and a linear curve can be fitted as shown in Fig. 4(a). The results of using the thrust meter to test the thrust of the motor show that at low voltage (velocity) the thrust is linear, while at high voltage (velocity), the thrust becomes a constant, as shown in Fig. 4(b). Therefore, the saturated thrust is the sliding friction, approximately equal to the break-away force of the static friction. The micro behavior of the motor is complex, and it is impossible to identify the other friction parameters without high-resolution test instruments.

2) The tracking errors caused by the static friction lead to the time delay and flat peak problems:

Jiasi Mo et al. have examined this ultrasonic linear motor with a simplified model, assuming that there is no relative sliding in the movement process. It is a system model containing no friction model. The experimental results demonstrate that omitting the friction model will not affect the point-to-point positioning accuracy but will markedly affect the trajectory tracking precision, as shown in Fig. 5

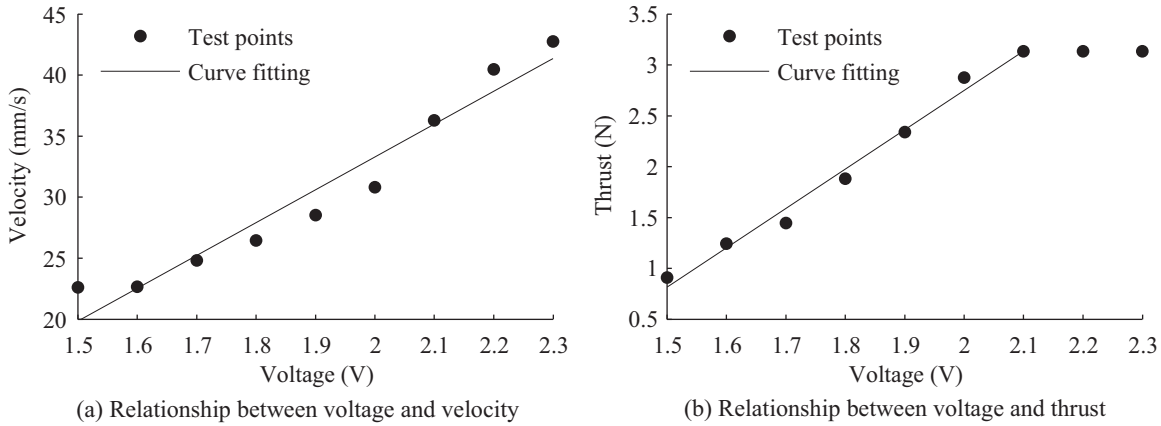

(a) Relationship between voltage and velocity (b) Relationship between voltage and thrust

Fig. 4. Experimental friction identification. (a) Relationship between voltage and velocity. (b) Relationship between voltage and thrust.

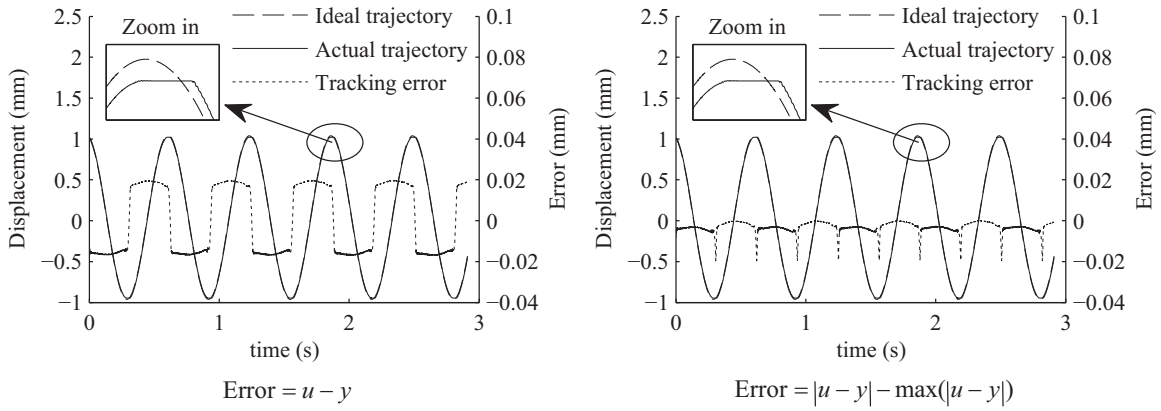

Fig. 5. Sine wave trajectory tracking and tracking error [28]. Error = $u - y$. Error = $|u - y| - \max(|u - y|)$.

[28]. This issue leads to time delay and flat peak problems in a low-velocity regime, especially during velocity reversals [5,28]. The trajectory tracking time delay and flat peak are the main sources of tracking error, caused by the static friction. To improve the trajectory tracking accuracy, friction compensation is needed.

The static friction is the thrust necessary to initiate motion from rest. It causes a region of zero output (zero velocity and zero displacement) for a nominal input to the motor (drive voltage) around any static null. Therefore, there is a dead-zone in which the motor will not respond. When the motor thrust is large enough to overcome the static friction, the motor will start to move. The command voltage required to overcome the static friction is called the break-away voltage.

Friction modeling can be complex, particularly in accounting for the details of friction around velocity reversals, at very low velocity or for very small motions. In this case, the ultrasonic linear motor positioning system produces a flat peak in the sine wave tracking, as shown in Fig. 6(a). Thus, a dead-zone phenomenon appears at low velocity, especially in velocity reversals. The dead-zone depth has been defined as the distance from the target wave peak to the actual flat peak. For essential dead-zone nonlinearity, the traditional PID linear control algorithm cannot compensate.

The dead-zone phenomenon usually takes place at low velocity, or in the velocity reversal regime. Therefore, it can be identified by applying different sine waves as the input signals to the system. Fig. 6(a) shows the definition of the dead-zone depth

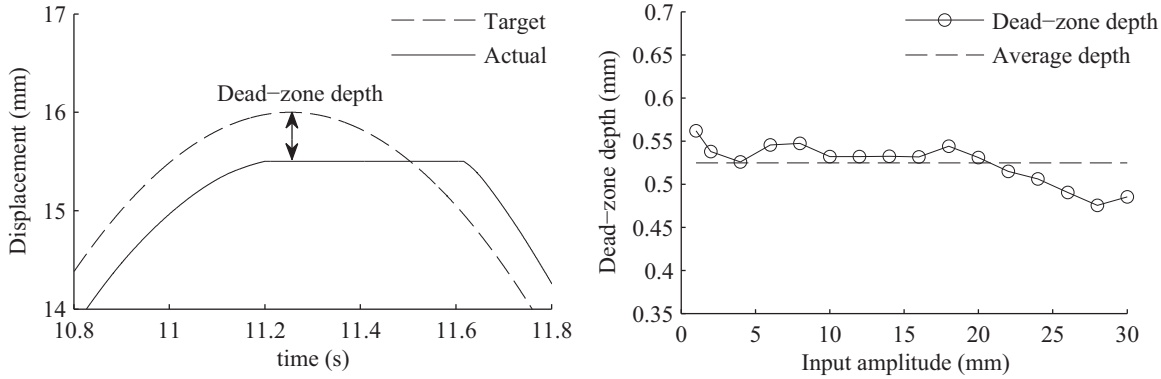

(a) Definition of the dead-zone depth (b) Dead-zone depth test

Fig. 6. Dead-zone test of the ultrasonic linear motor positioning system. (a) Definition of the dead-zone depth. (b) Dead-zone depth test.

when applying a sine wave of 16.00 mm amplitude. The depth of the dead-zone is tested as shown in Fig. 6(b). When applying sine wave voltages with the same frequency but different amplitudes to the positioning system, the magnitude of the dead-zone is nearly the same, approximately 0.52 mm, as shown in Fig. 6, which means that it is caused by the break-away force of the static friction.

3. Constant feedforward with an integral separation PID control

Due to system uncertainty, the friction model is difficult to model. The dead-zone of the static friction is stable, as shown in Fig. 6. Therefore, it is feasible to compensate for it through the feedforward method. This section addresses the system modeling and simulation of the constant feedforward with an integral separation PID.

3.1. System modeling

The ultrasonic linear motor is a U-264 PI made in Germany. The prior knowledge of the motor is limited for three reasons. First, this motor is a product packed in a case, so it is impossible to know the structure inside the motor. Second, even if the motor is unpacked to show the inside structure, the parameters of the PZT are still unknown. The third reason is that the ultrasonic linear motor is a complex electromechanical system, and the motion of the motor is based on the drive signal. We can only test the input and output signal of the motor drive board. It is difficult to determine the relationship between the input signal and the motion of the motor, so it is very difficult to model the motor accurately. Jiasi Mo used a simplified model to describe the ultrasonic linear motor, but it is not suitable for control because there are some unknown parameters [28].

To address the problem of the modeling difficulty, an experimental method that treats the system as a black box can obtain the relationship between the input and output. For an open-loop system, the input signal is the DC reference voltage (-10 V $\sim$ $+10$ V), and the output is the velocity or displacement (velocity integral) of the motor. For the closed-loop positioning, the input signal is the targeted position, and the output is the actual position.

This frequency response method is used to identify the system model through sine wave inputs with different frequency. The frequency response curve and the fitting curve of the magnitude and frequency characteristics are plotted in Fig. 7. For the open-loop case, the input is a voltage signal, and the output is the displacement. For the closed-loop case, the input and output are both displacement.

The order of the transfer function can be obtained via the experimental Bode plot. According to the open-loop magnitude frequency characteristic curve, as shown in Fig. 7(a), the slope of the low-frequency response is -20 dB, proving that there is an integration element, and there is a small peak near the corner frequency. After the corner frequency, the slope changes to -60 dB, proving that there is a second-order oscillation element. In combination with these two elements, the open-loop transfer function becomes a third-order system when the output is the displacement signal. According to the closed-loop magnitude frequency characteristic curve, as shown in Fig. 7(b), the slope of the low frequency response is 0 dB; after the corner frequency, the slope changes to -40 dB. The order of the system transfer function changes to 2 from 3 after the unit negative feedback, proving that the transfer function of the system has one zero point. If the output is velocity, the open-loop system is simply a second-order oscillation element. Because the ultrasonic linear motor positioning system is a positioning device, the displacement is of interest. The open-loop system is a third-order system, and the fitting transfer function is

$$\frac{K(as+1)}{s(\frac{s^2}{\omega^2}+2\xi\frac{s}{\omega}+1)}, \tag{1}$$

where $K=2.82$ is the open-loop gain; $\omega=210$ is the corner frequency; $\xi=0.45$ is the damping factor; a=0.001.

After applying unit feedback, the open-loop system Eq. (1) takes the form

$$\frac{b_0 s+b_1}{a_0 s^3+a_1 s^2+a_2 s+a_3} \tag{2}$$

Because a_0 is much less than a_1, the third-order item can be ignored, making the unit feedback system

$$\frac{b_0 s+b_1}{a_1 s^2+a_2 s+a_3} \tag{3}$$

where $b_0=9.5$, $b_1=950$, $a_0\approx 0$, $a_1=1$, $a_2=76.8$, $a_3=1024$.

The frequency response of the closed loop system is shown in Fig. 7(b).

3.2. Simulation

The PID control algorithm is a linear and model-free control method. It is simple but has a good control effect, so it is widely used in positioning and some other situations. The PID control

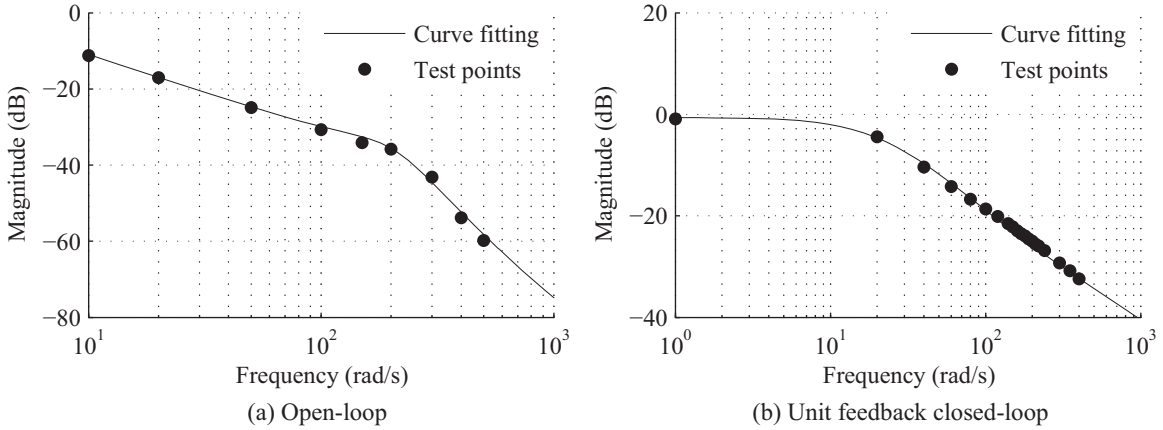

Fig. 7. Curve fitting of magnitude and frequency characteristics. (a) Open-loop. (b) Unit feedback closed-loop.

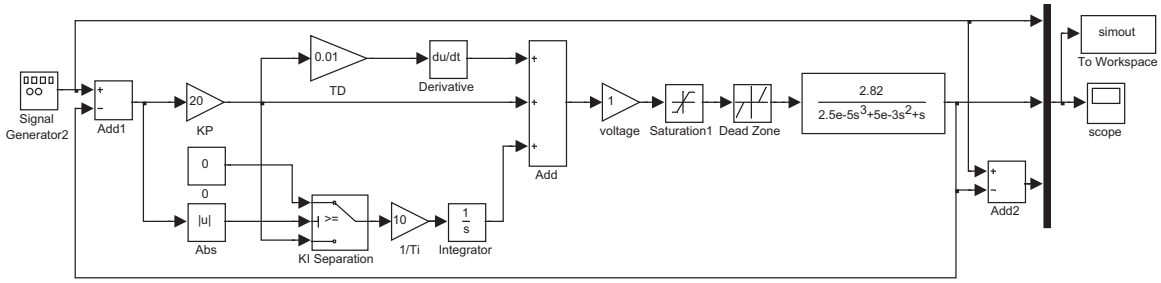

Fig. 8. Integral separation PID control diagram ($K_p=20$, $1/T_i=10$, $T_d=0.01$, $e_{threshold}=1.00$ mm).

algorithm can compensate for weak nonlinearity, although it is a linear control method. However, the PID control algorithm is not suitable for very precise motion control because it cannot compensate for nonlinear phenomena such as backlash and dead-zone. This paper investigates an improved PID algorithm called constant feedforward with the integral separation PID. It consists of the feedback element of the integral separation PID and the feedforward element of the static friction compensation.

The integral separation PID control algorithm is expressed as Eq. (4), where $u(k)$ is the command voltage at moment kT, calculated from the feedback error $e(k)$, and x_a is the actual output of the system. The main design parameters of the PID controller are control gain K_p, integration time T_i and differential time T_d.

$$\begin{cases} u(k) = K_p e(k)[1 + T_d[x_a(k) - x_a(k-1)] + \dfrac{1}{T_i}\sum_{j=0}^{k-1} e(j)] \\ \dfrac{1}{T_i} = 0; \quad (e(k) > e_{threshold}) \end{cases} \tag{4}$$

To prevent an excessive amount of overshoot caused by the integral action, the integral separation PID algorithm is adopted. When the feedback deviation is less than the threshold, the integral action is introduced to minimize the residual error. When the feedback deviation $e(k)$ is larger than the threshold $e_{threshold}$, only the PD control is used.

A block diagram is built in SIMULINK/MATLAB to simulate the control algorithm, as shown in Fig. 8. The system simulation uses the identified transfer function (1) as the ultrasonic linear motor positioning system. The input signal is a sine wave with 1 mm amplitude and πrad/s frequency. After tuning, the parameters are selected as $K_p=20$, $1/T_i=10$, $T_d=0.01$, $e_{threshold}=1.00$ mm, and the sample time is 0.001 s. In the simulation, the dead-zone is set to 0.50 mm based on Fig. 6.

Without the feedforward compensation, the simulation result of applying the sine wave signal as the input signal to the system and using only the integral separation PID algorithm is shown in Fig. 9. The result is similar to Fig. 5, with the time delay and flat peak.

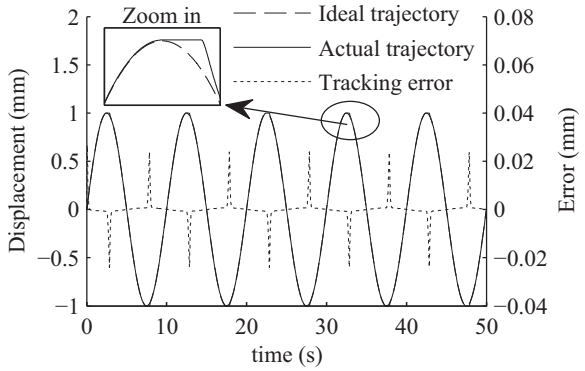

Fig. 9. The simulation result without compensation.

Fig. 9 shows that the integral separation PID algorithm cannot compensate for the dead-zone caused by the static friction, although the time delay can be decreased. The flat peak remains. The dead-zone depth has already been identified experimentally, as shown in Fig. 6. Fig. 9 shows that the simulation with a dead-zone element obtains a similar result. These coincidences show that the static friction effect can be approximated by a dead-zone. A simple way to compensate for the static friction is to implement a fast crossing through the dead zone [4], which can be accomplished using a feedforward compensator, as shown in Fig. 10.

When the motor moves inside the dead-zone due to the static friction, the more time is spent inside it, the more errors are produced. To reduce the time inside the dead-zone, a constant compensation value equal to the depth of the dead-zone must be added (or subtracted, depending on the motion direction) to the PID command voltage when the position approaches the dead-zone. The compensation direction can be obtained by computing the sign of the velocity. The main idea of this constant value compensator is to avoid the dead-zone or at least minimize the time spent in it. The whole mathematical expression of this compensation strategy can be expressed as

$$\begin{cases} u(k) = K_p e(k)[1 + T_d[x_a(k) - x_a(k-1)] + \dfrac{1}{T_i}\sum_{j=0}^{k-1} e(j)] \\ \quad + V_{compensate}\,\mathrm{sign}(x_d'(k)) \\ \dfrac{1}{T_i} = 0; \; (e(k) > e_{threshold}) \end{cases} \tag{5}$$

In Eq. (3), $x_d'(k)$ denotes the desired velocity of the input. The sign function determines the compensation direction. $V_{compensate}$ is the compensation value related to the dead-zone caused by the static friction. When the system is near or in the dead-zone, the feedforward value can make the system cross the dead-zone more quickly and reduce the time remaining in it. In other words, this constant value can compensate for the steady errors caused by the static friction. The simulation results are shown in Fig. 11. Comparing Fig. 9 with Fig. 11 shows that this compensator can reduce errors and eliminate the flat peak phenomenon. The comparison of the errors is shown in Fig. 12.

4. Adaptive feedback and feedforward control algorithms

Although the constant feedforward with the integral separation PID control can reduce errors and the flat peak phenomenon, it is unable to compensate effectively for the uncertainty of the system. The uncertainty of this system includes the asymmetrical friction interface and the environmental disturbance described in Section 2, making the system a slow-time-varying system. The control algorithm described in Section 3 is limited in its ability to compensate for static friction because the feedforward value of the voltage is a certain value, without adaptability. Thus, the control

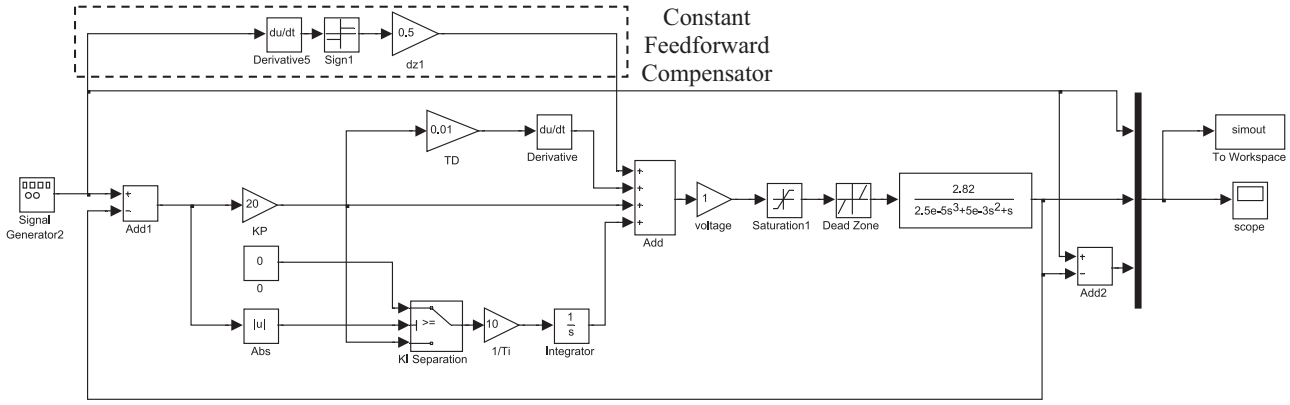

Fig. 10. Diagram of the integral separation PID control with constant value compensation.

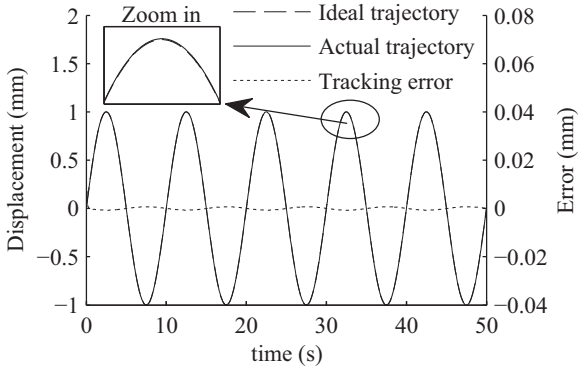

Fig. 11. The simulation results with compensation.

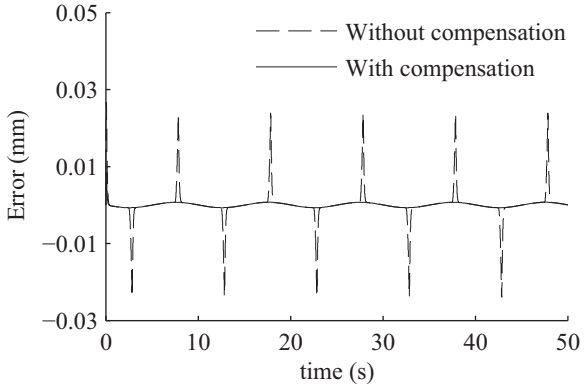

Fig. 12. Comparison of simulation errors.

algorithm introduced in Section 3 is suitable only for the situation of the steady friction state and invariable friction parameters. If the system is a time-varying system, or the uncertainty of the system is remarkable, the constant value compensator is obviously not sufficient. Aiming at this problem, this section adopts an adaptive compensation algorithm to improve the trajectory tracking accuracy. The compensation value will be adjusted adaptively.

4.1. System identification

The model reference adaptive control (MRAC) is used to perform the trajectory tracking and friction compensation. The MRAC cannot work without the reference model. The reference model is used to describe the desired input/output of the closed-loop system. The MRAC seeks a type of control law to make the performance of the closed-loop system fully track the performance of the reference model. Therefore, the design objective of the MRAC system includes two main aspects: one is to establish a reference model, and the other is to derive an adaptive law.

The MRAC system is often associated with system identification because the reference model is usually the identification model of the system [31]. As mentioned in Section 2, this ultrasonic linear motor positioning system is difficult to model theoretically. System identification is required. The identification model is a linear model approximating the actual system. Because the system characteristics are similar, the adaptive law converges easily, and it can compensate for the nonlinearity.

The identification model is used as the system reference model via the least square method according to the least square principle by minimizing the generalized deviation of the sum of the squares to determine the parameters of the system model. The least square method is divided into offline and online least squares. Considering the real-time and control accuracy of the system, an online method must be adopted. The forgetting factor recursive least square (FFRLS) method is used to identify the system model. Because the forgetting factor can overcome the data saturation, it is suitable for identifying the time-varying system.

The RLS form is written as

$$\text{New estimate } \hat{\boldsymbol{\theta}}(k) = \text{Old estimate } \hat{\boldsymbol{\theta}}(k-1) + \text{Correction}. \tag{6}$$

The estimation of the least square in moment k is

$$\hat{\boldsymbol{\theta}}(k) = (\boldsymbol{\Phi}_k^T \boldsymbol{\Phi}_k)^{-1} \boldsymbol{\Phi}_k^T \mathbf{Y}_k \tag{7}$$

where $\boldsymbol{\Phi}_k = \begin{Bmatrix} \boldsymbol{\Phi}_{k-1} \\ \boldsymbol{\varphi}^T(k) \end{Bmatrix} \in \mathbf{R}^{k\times(n_a+n_b+1)}$, $\mathbf{Y}_k = \begin{pmatrix} \mathbf{Y}_{k-1} \\ y(k) \end{pmatrix} \in \mathbf{R}^{k\times 1}$, $\boldsymbol{\varphi}(k)$ is a data vector, n_a, n_b are the order numbers of the system, and $\mathbf{Y}(k)$is the output vector.

Let

$$\begin{aligned} \mathbf{P}(k) &= (\boldsymbol{\Phi}_k^T \boldsymbol{\Phi}_k)^{-1} = [\boldsymbol{\Phi}_{k-1}^T \boldsymbol{\Phi}_{k-1} + \boldsymbol{\varphi}(k)\boldsymbol{\varphi}^T(k)]^{-1} \\ &= [\mathbf{P}^{-1}(k-1) + \boldsymbol{\varphi}(k)\boldsymbol{\varphi}^T(k)]^{-1}, \end{aligned} \tag{8}$$

There is

$$\mathbf{P}^{-1}(k) = \mathbf{P}^{-1}(k-1) + \boldsymbol{\varphi}(k)\boldsymbol{\varphi}^T(k). \tag{9}$$

Considering Eq. (7), this equation yields

$$\hat{\boldsymbol{\theta}}(k-1 = \left(\boldsymbol{\Phi}_{k-1}^T \boldsymbol{\Phi}_{k-1}\right)^{-1} \boldsymbol{\Phi}_{k-1}^T \mathbf{Y}_{k-1} = \mathbf{P}(k-1)\boldsymbol{\Phi}_{k-1}^T \mathbf{Y}_{k-1}. \tag{10}$$

Combining Eqs. (9) and (10), one can obtain

$$\boldsymbol{\Phi}_{k-1}^T \mathbf{Y}_{k-1} = \mathbf{P}^{-1}(k-1)\hat{\boldsymbol{\theta}}(k-1 = \left[\mathbf{P}^{-1}(k) - \boldsymbol{\varphi}(k)\boldsymbol{\varphi}^T(k)\right]\hat{\boldsymbol{\theta}}(k-1). \tag{11}$$

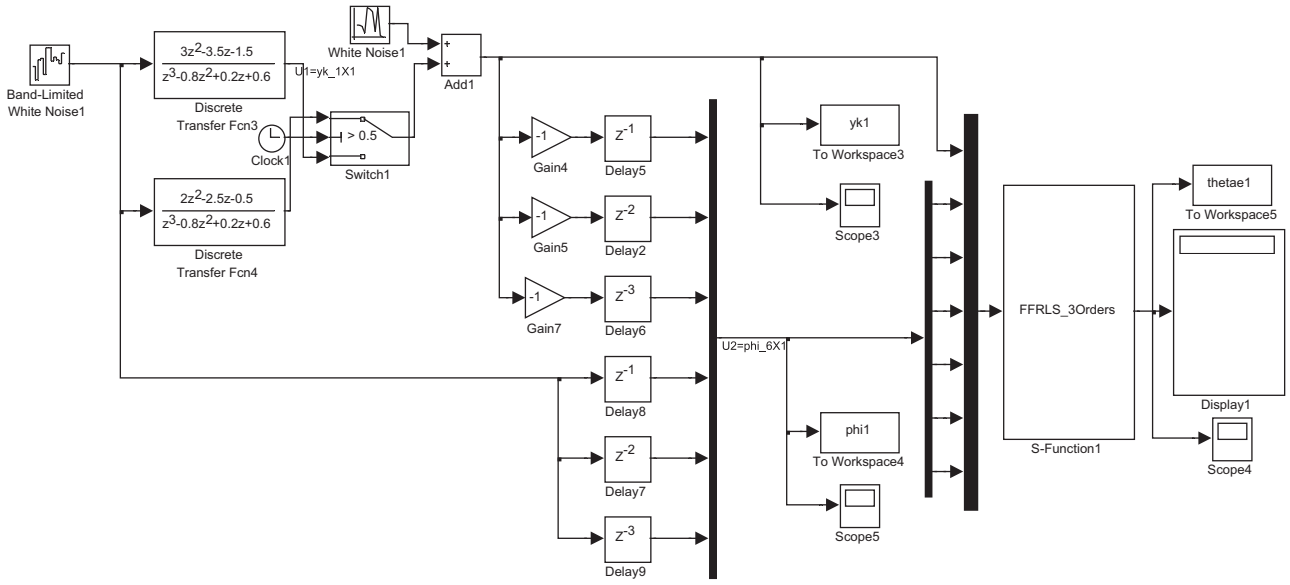

Fig. 13. Simulation diagram of the RLS.

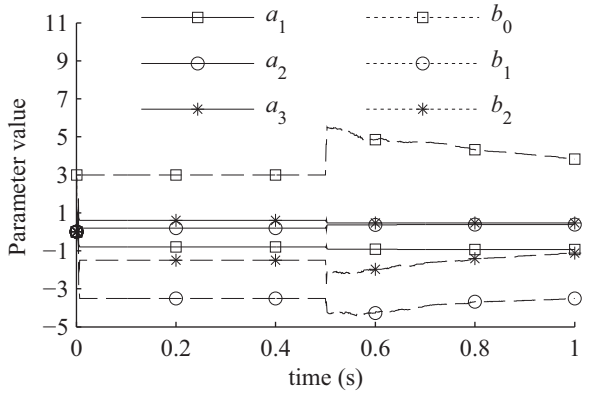

Fig. 14. The updating of the $\hat{\boldsymbol{\theta}}(k)$ using the RLS.

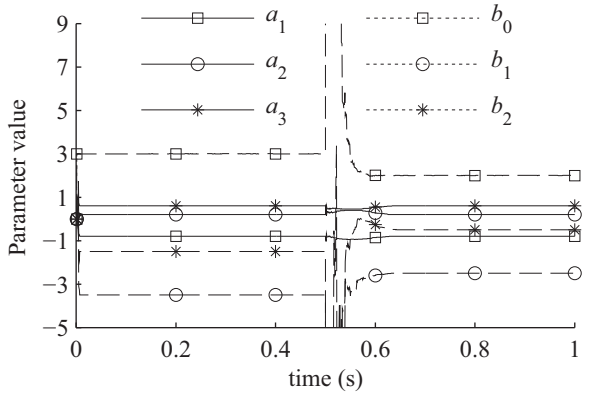

Fig. 15. The updating of $\hat{\boldsymbol{\theta}}(k)$ using the FFRLS.

Thus, Eq. (6) can be written as

$$\hat{\boldsymbol{\theta}}(k) = \hat{\boldsymbol{\theta}}(k-1) + \mathbf{K}(k)[y(k) - \boldsymbol{\varphi}^T(k)\hat{\boldsymbol{\theta}}(k-1)], \tag{12}$$

where $\mathbf{K}(k) = \mathbf{P}(k)\boldsymbol{\varphi}(k)$.

According to the matrix inversion lemma, $\mathbf{K}(k)$ and $\mathbf{P}(k)$ can be obtained. The RLS can be expressed as

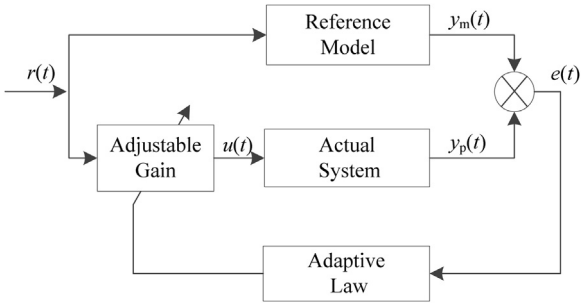

Fig. 16. The traditional MRAC control block diagram.

$$\begin{cases} \hat{\boldsymbol{\theta}}(k) = \hat{\boldsymbol{\theta}}(k-1) + \mathbf{K}(k)[y(k) - \boldsymbol{\varphi}^T(k)\hat{\boldsymbol{\theta}}(k-1)] \\ \mathbf{K}(k) = \dfrac{\mathbf{P}(k-1)\boldsymbol{\varphi}(k)}{1 + \boldsymbol{\varphi}^T(k)\mathbf{P}(k-1)\boldsymbol{\varphi}(k)} \\ \mathbf{P}(k) = [I - \mathbf{K}(k)\boldsymbol{\varphi}^T(k)]\mathbf{P}(k-1) \end{cases}. \tag{13}$$

Eq. (13) is the RLS method used to identify the system, and n_a and n_b must be determined beforehand. According to the experimental results shown in Fig. 7, choosing $n_a = 3$, $n_b = 2$, the system difference equation is written as

$$\begin{aligned} y(k) = &- a_1 y(k-1) - a_2 y(k-2) - a_3 y(k-3) + b_0 u(k-1) \\ &+ b_1 u(k-2) + b_2 u(k-3) + \xi(k) \end{aligned} \tag{14}$$

where $y(k)$ is the output; $u(k)$ is the input; and $\xi(k)$ is the noise. After using the Z transform, the discrete transfer function is

$$G(z) = \frac{b_0 z^2 + b_1 z + b_2}{z^3 + a_1 z^2 + a_2 z + a_3} \tag{15}$$

Using Eq. (15) as the system structure, a simulation is performed to test the performance of the RLS method in identifying the system parameters' variation. The time-varying system used to test the RLS method is

$$\begin{cases} G(z) = \dfrac{3z^2 - 3.5z - 1.5}{z^3 - 0.8z^2 + 0.2z + 0.6}, & t \le 0.5\text{s} \\ G(z) = \dfrac{2z^2 - 2.5z - 0.5}{z^3 - 0.8z^2 + 0.2z + 0.6}, & t > 0.5\text{s} \end{cases}. \tag{16}$$

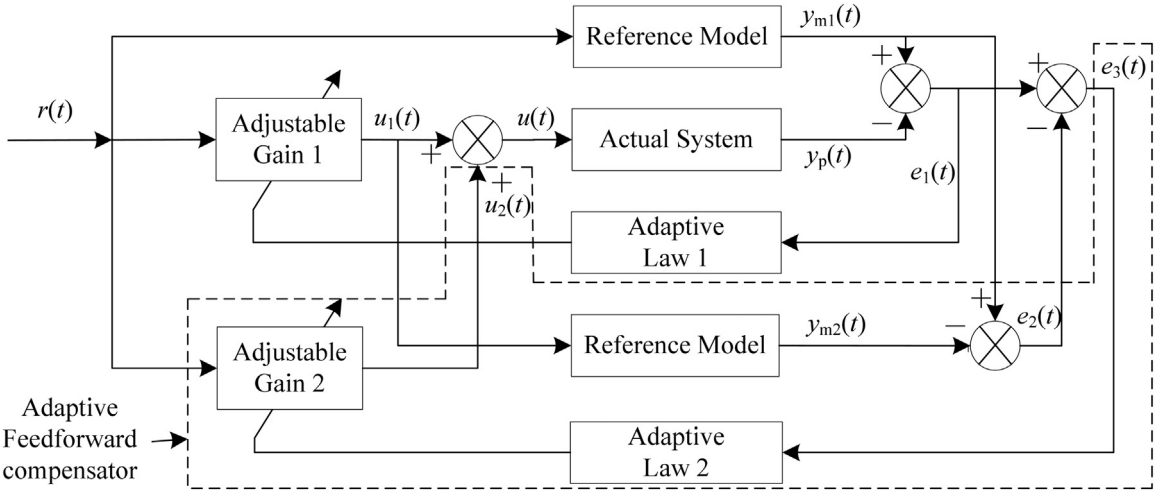

Fig. 17. Adaptive feedback and feedforward control block diagram.

The simulation block diagram is illustrated in Fig. 13. The RLS method is written as an S-function in SIMULINK/MATLAB.

The simulated input vector is $\boldsymbol{\varphi}(k)$; the estimated output value is $\hat{\boldsymbol{\theta}}(k)$. The updating parameters of $\hat{\boldsymbol{\theta}}(k)$ are plotted in Fig. 14. Without noise in the simulation, the RLS method is an unbiased estimation. Fig. 14 shows that $\hat{\boldsymbol{\theta}}(k)$ is the same as Eq. (16) when $t \le 0.5$s. However, there is a large deviation when $t > 0.5$s because of a sudden change in the system. This phenomenon is called data saturation, where the new information on the system cannot modify $\hat{\boldsymbol{\theta}}(k)$ effectively.

The ultrasonic linear motor positioning system is a slow-time-varying system, so the RLS method is not very good for identifying it. Hence, the forgetting factor is introduced into the RLS, called FFRLS, with the capability to identify the time-varying system. The FFRLS is written as

$$\begin{cases} \hat{\boldsymbol{\theta}}(k) = \hat{\boldsymbol{\theta}}(k-1) + \mathbf{K}(k)[y(k) - \boldsymbol{\varphi}^T(k)\hat{\boldsymbol{\theta}}(k-1)] \\ \mathbf{K}(k) = \dfrac{\mathbf{P}(k-1)\boldsymbol{\varphi}(k)}{\lambda + \boldsymbol{\varphi}^T(k)\mathbf{P}(k-1)\boldsymbol{\varphi}(k)} \\ \mathbf{P}(k) = \dfrac{1}{\lambda}[I - \mathbf{K}(k)\boldsymbol{\varphi}^T(k)]\mathbf{P}(k-1) \end{cases} \tag{17}$$

where λ is the forgetting factor.

The forgetting factor λ can update the data and weaken the data saturation phenomenon. It is usually selected between 0.9 and 1. If $\lambda = 1$, the FFRLS becomes the RLS.

The results of introducing the FFRLS into the simulation (Fig. 13) are shown in Fig. 15. The results show that $\hat{\boldsymbol{\theta}}(k)$ converges quickly, and $\hat{\boldsymbol{\theta}}(k)$ is the same as Eq. (16) after introducing $\lambda = 0.9$.

4.2. Adaptive control law

Without considering nonlinearity, the identified model of the system is linear. It is used as the reference system to reduce the effect of the nonlinearity. The key to designing the MRAC is to search for the adaptive law, which minimizes the generalized deviation between the reference model and the actual system. The traditional MRAC control block diagram is shown in Fig. 16, where $e(t)$ is defined as the generalized deviation, i.e., the difference between the output $y_m(t)$ and $y_p(t)$, namely, $e(t) = y_m(t) - y_p(t)$. The function of the adaptive law is to minimize $e(t)$ by adjusting the parameters of the system. Therefore, $u(t)$ is adaptively updated, and $e(t)$ tends to zero. However, the actual system is a nonlinear system containing a dead-zone. When the control signal $u(t)$ is too small or changes direction, the system will not respond due to the existence of the dead-zone.

The MRAC feedback control law alone cannot eliminate the dead-zone nonlinearity. To address this problem, in combination with the results of Section 3, the adaptive feedforward method is utilized. The adaptive friction compensation control algorithm is combined with the MRAC feedback and feedforward control. The compensation value is adaptively modified according to the volume of the dead-zone, so it can reduce the influence of the system uncertainty as far as possible.

The compensation value of the feedforward is also relative to $e(t)$, but it is not calculated solely from $e(t)$ but from the generalized deviation. The control block diagram is shown in Fig. 17.

The control value $u(t) = u_1(t) + u_2(t)$ consists of the feedback $u_1(t)$ and the feedforward control value $u_2(t)$, where $u_1(t)$ is the basic signal of the tracking control, and $u_2(t)$ is the friction compensation value. Due to the effect of adaptive law 1, the actual system can track the output of the reference model and minimize the generalized deviation $e_1(t) = y_{m1}(t) - y_p(t)$. Because the reference model is linear, the control effect $u_1(t)$ is linear. Thus, it is unable to compensate for the dead-zone phenomenon of the actual system. When $u_1(t)$ operates on the actual system, the system output shows the dead-zone features as a flat peak. Because $u_1(t)$ is not sufficient to control the system well, $e_2(t)$ is defined as $e_2(t) = y_{m1}(t) - y_{m2}(t)$. Although $y_{m1}(t)$ and $y_{m2}(t)$ are the outputs of the same reference model, the inputs are different: $y_{m1}(t)$ corresponds to $r(t)$, and $y_{m2}(t)$ corresponds to $u(t)$. Here, $e_2(t)$ is the generalized tracking error with no dead-zone. Then, define $e_3(t) = e_1(t) - e_2(t)$. Because $e_1(t)$ is the generalized tracking error with dead-zone, $e_3(t)$ is the steady state error caused by the dead-zone. That is to say, the amplitude of $e_3(t)$ is the dead-zone depth, and the phase of $e_3(t)$ is the dead-zone action time. Therefore, if adaptive law 2 can minimize $e_3(t)$, the dead-zone will be compensated.

The key to designing this control algorithm is to seek the adaptive law to realize the blocks of adaptive law 1 and adaptive law 2. To guarantee the system will be globally asymptotically stable, adaptive law 1 and 2 are designed via Lyapunov's method. The implementation methods of adaptive law 1 and 2 are consistent. Because only the parameters are different, only adaptive law 1 needs to be derived.

In 1966, the German scholar P. C. Parks used Lyapunov's stability theory to design the MRAC [32]. The key problem is to construct a proper Lyapunov function and then determine the adaptive law to guarantee that the derivative of the Lyapunov function is negative definite or negative semi-definite. This

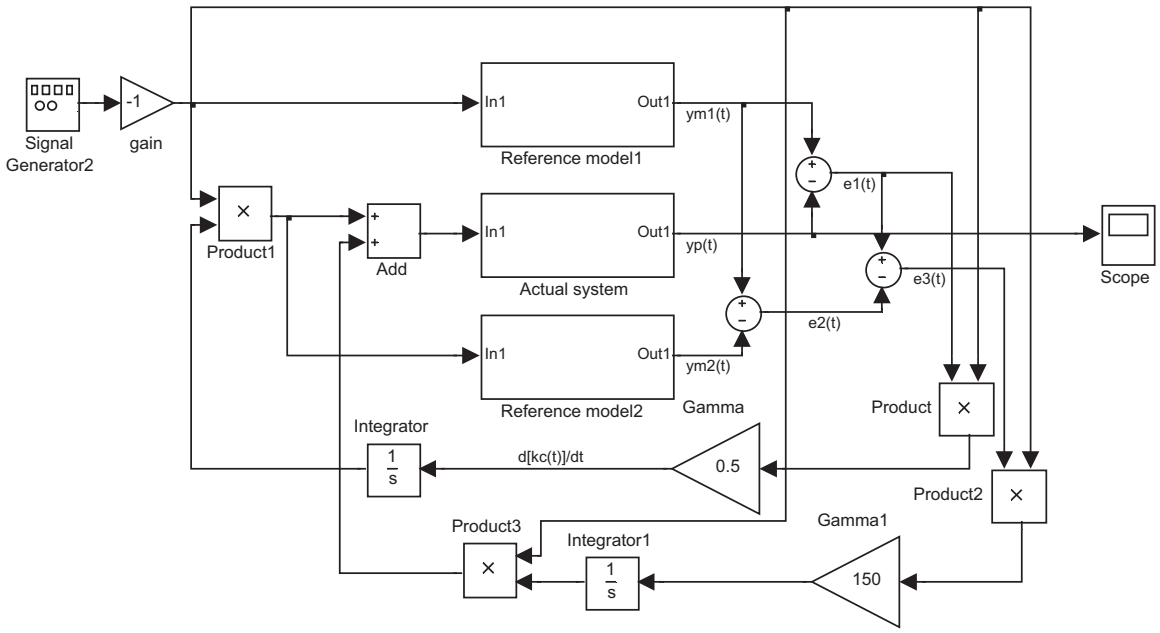

Fig. 18. Simulation block diagram.

approach ensures the stability of the system and a high adaptive rate. The adjustable gain adaptive law is written as follows.

Assuming the transfer function of the control object is

$$G(z) = K_v \frac{N(z)}{D(z)}, \tag{18}$$

the transfer function of the reference model is

$$G(z) = K_m \frac{N(z)}{D(z)}, \tag{19}$$

where $D(z) = z^n + a_1 z^{n-1} + \ldots + a_{n-1} z + a_n$, and $N(z) = b_1 z^{n-1} + \ldots + b_{n-1} z + b_n$; the coefficients a_i, b_i are obtained by identification; and K_m is the ideal model gain.

The gain K_v is a slow-time-varying parameter, which makes the controller an adjustable parameter to compensate for K_v

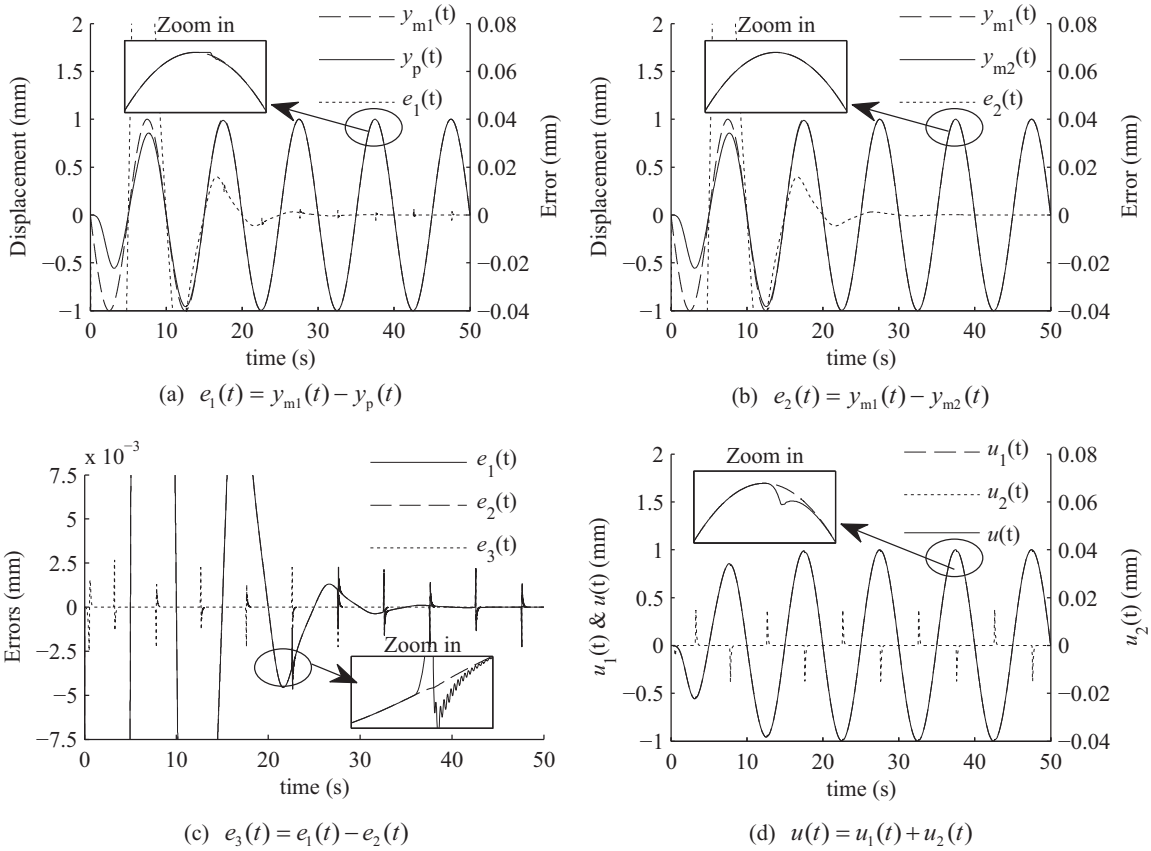

Fig. 19. Simulation signals. (a) $e_1(t) = y_{m1}(t) - y_p(t)$. (b) $e_2(t) = y_{m1}(t) - y_{m2}(t)$. (c) $e_3(t) = e_1(t) - e_2(t)$. (d) $u(t) = u_1(t) + u_2(t)$.

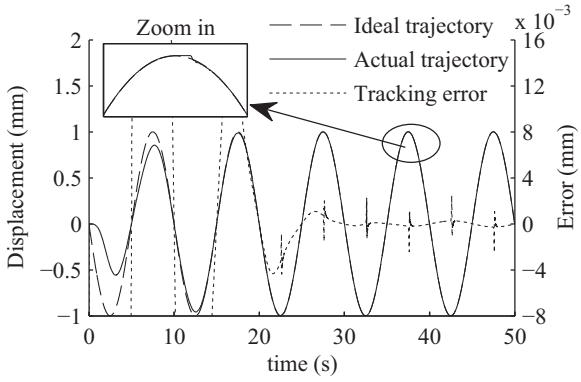

Fig. 20. Simulation result of the adaptive feedback and feedforward control algorithm.

$$w_s(z) = K_c. \tag{20}$$

At the initial moment, $K_cK_v \neq K_m$, so there is a generalized deviation $e = y_m - y_p$. The purpose of the design is to adjust K_c, ensuring that

$$\begin{cases} \lim\limits_{t\to\infty} e(t) = 0 \\ \lim\limits_{t\to\infty} (K_m - K_cK_v) = 0 \end{cases}. \tag{21}$$

From Eqs. (19) and (18), one can obtain a generalized error difference equation as

$$\begin{cases} e^{(n)} + a_1e^{(n-1)} + \ldots + a_{n-1}\dot{e} + a_ne \\ \quad = K(b_1r^{(n-1)} + \ldots + b_{n-1}\dot{r} + b_nr) \\ K = K_m - K_cK_v \end{cases}. \tag{22}$$

The derivative of K is

$$\dot{K} = -K_v\dot{K}_c. \tag{23}$$

The generalized error equation is converted into a standard state space form as

$$\begin{cases} \dot{\varepsilon} = \mathbf{A}\varepsilon + K_cr \\ e = \mathbf{h}^T\varepsilon \end{cases}. \tag{24}$$

The state variables are chosen as

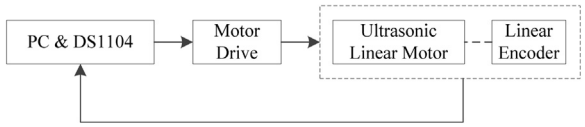

Fig. 22. Block diagram of the closed-loop system.

$$\begin{cases} \varepsilon_1 = e \\ \varepsilon_2 = \dot{\varepsilon}_1 - c_1r \\ \varepsilon_3 = \dot{\varepsilon}_2 - c_2r \\ \vdots \\ \varepsilon_n = \dot{\varepsilon}_{n-1} - c_{n-1}r \end{cases}. \tag{25}$$

Thus,

$$\varepsilon = [\varepsilon_1, \varepsilon_2, \ldots, \varepsilon_n]^T = [e, \dot{e} - c_1r, \ldots, e^{(n-1)} - c_{n-1}r]^T. \tag{26}$$

$$\begin{cases} \mathbf{A} = \begin{bmatrix} 0 & I_{n-1} \\ -a_n & -a_{n-1}\ldots - a_1 \end{bmatrix} \\ \mathbf{c} = \begin{bmatrix} c_1 \\ c_2 \\ \vdots \\ c_3 \end{bmatrix} = \begin{bmatrix} 1 & 0 & \cdots & 0 \\ a_1 & 1 & \cdots & 0 \\ a_2 & a_1 & 1\ 0\ 0 & \\ \vdots & \vdots & \ddots & \\ a_{n-1} & a_{n-2} & \cdots & 1 \end{bmatrix} \begin{bmatrix} b_1 \\ b_2 \\ \vdots \\ b_n \end{bmatrix} \\ \mathbf{h}^T = [1\ \ 0\ \ \ldots\ \ 0] \end{cases}. \tag{27}$$

Composed of the state variable ε and the adjustable gain K_c, an augmented state space Lyapunov function is defined as

$$V = \varepsilon^T\mathbf{P}\varepsilon + \lambda\mathbf{K}^2. \tag{28}$$

where $\mathbf{P}$ is a symmetric positive definite matrix, and $\lambda \geq 0$.

The derivation of the Lyapunov function V with respect to time t is

$$\dot{V} = \varepsilon^T(\mathbf{PA} + \mathbf{A}^T\mathbf{P})\varepsilon + 2\varepsilon^T\mathbf{P}crK + 2\lambda\mathbf{K}\dot{\mathbf{K}}. \tag{29}$$

Let $\mathbf{PA} + \mathbf{A}^T\mathbf{P} = -\mathbf{I}$. Then, $\varepsilon^T(\mathbf{PA} + \mathbf{A}^T\mathbf{P})\varepsilon$ is negative definite when $2\varepsilon^T\mathbf{P}crK + 2\lambda\mathbf{K}\dot{\mathbf{K}} = 0$. The system is stable in the sense of Lyapunov. The adaptive law is derived as

$$\dot{K}_c = \frac{1}{K_v\lambda}\varepsilon^T\mathbf{P}cr. \tag{30}$$

Let

$$\mathbf{P}c = \mathbf{h}\mu,\ \mu > 0. \tag{31}$$

Substituting Eqs. (31) into (30), the adaptive law does not contain the derivative error, as

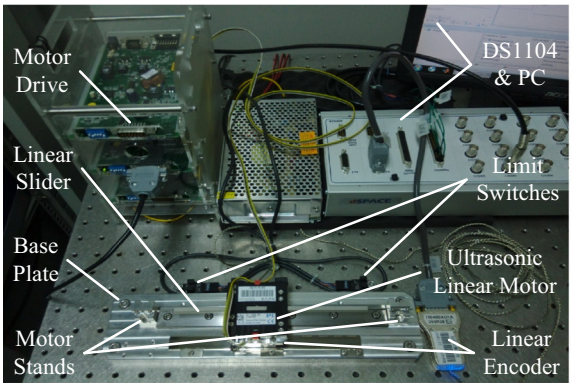

(a) Ultrasonic linear motor positioning system

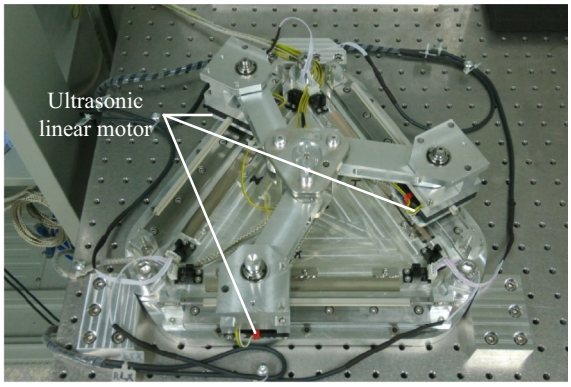

(b) 3PRR driven by ultrasonic linear motors

Fig. 21. Photographs of the experimental setups. (a) Ultrasonic linear motor positioning system. (b) 3PRR driven by ultrasonic linear motors.

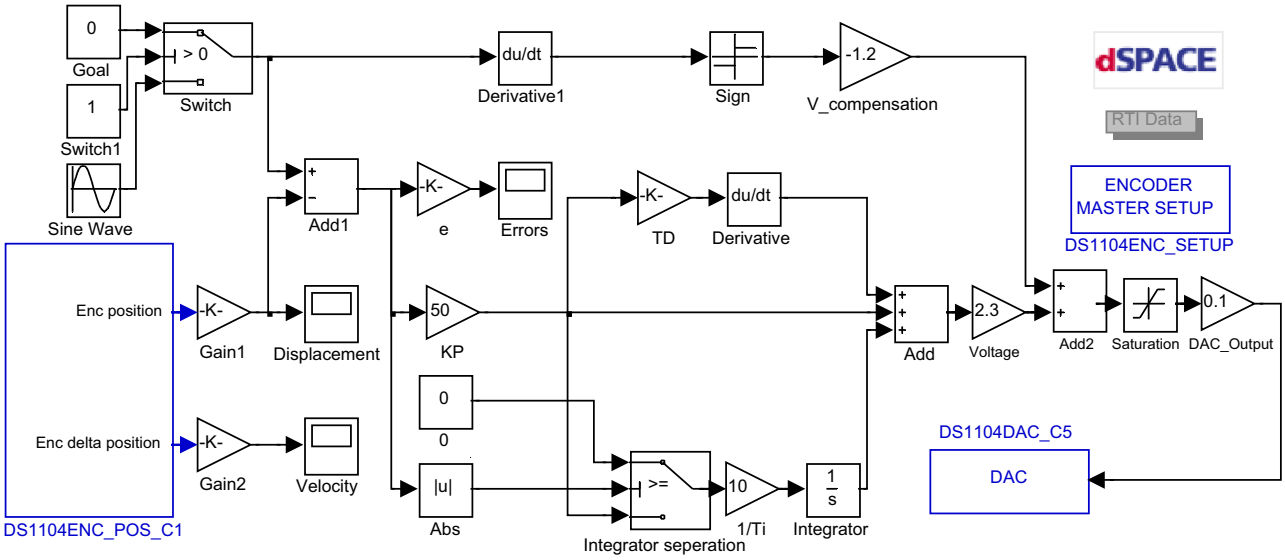

Fig. 23. The experimental control block diagram of the constant feedforward with integral separation PID.

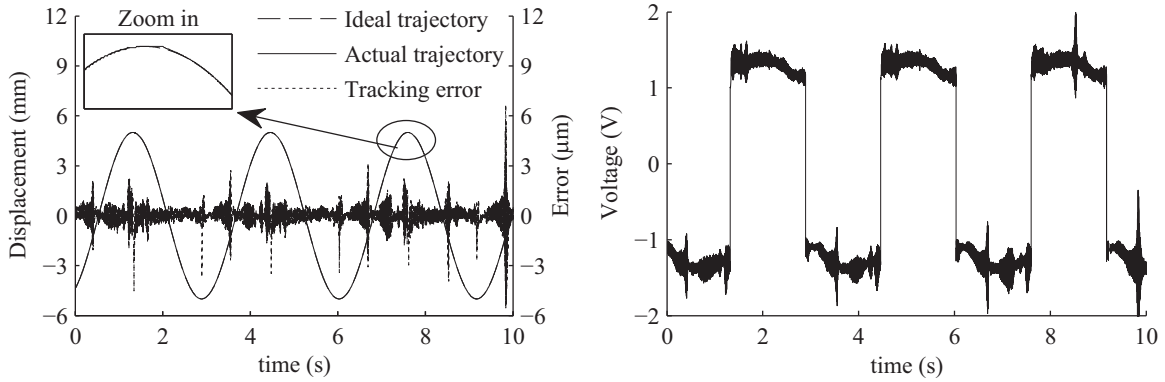

(a) The sine wave tracking result (b) The control voltage output from DS1104

Fig. 24. Sine wave tracking with amplitude 5 mm and frequency 2 rad/s. (a) The sine wave tracking result. (b) The control voltage output from DS1104.

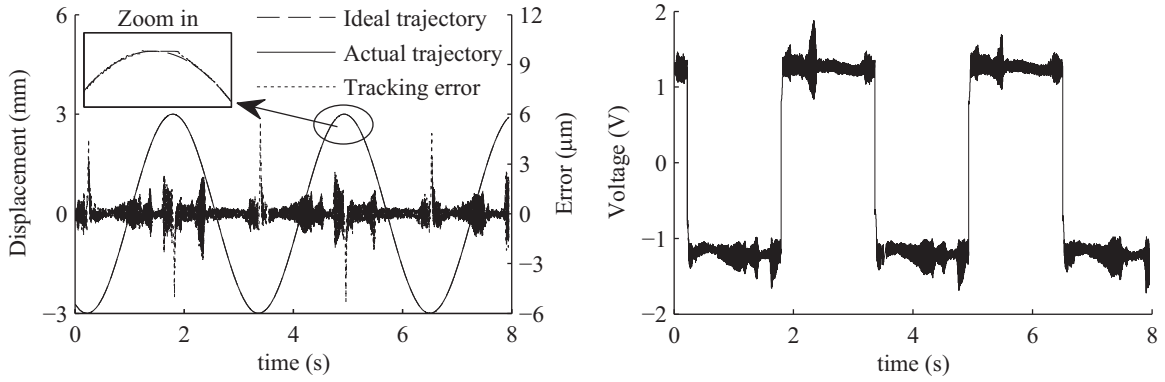

(a) The sine wave tracking result (b) The control voltage output from DS1104

Fig. 25. Sine wave tracking with amplitude 3 mm and frequency 2 rad/s. (a) The sine wave tracking result. (b) The control voltage output from DS1104.

$$\begin{cases} \dot{K}_c = \gamma e r \\ \gamma = \dfrac{\mu}{K_v \lambda} \end{cases}. \tag{32}$$

This adaptive law can be used like the block adaptive law 1 and law 2 in Fig. 17, but the parameter γ is different.

4.3. Simulation

A block diagram of SIMULINK/MATLAB is built in Fig. 17 to simulate the control algorithm Section 4.2. The simulation block diagram is shown in Fig. 18.

The reference models 1 and 2 are Eq. (1) with unity feedback, without a dead-zone. The actual system is also Eq. (1) but with a

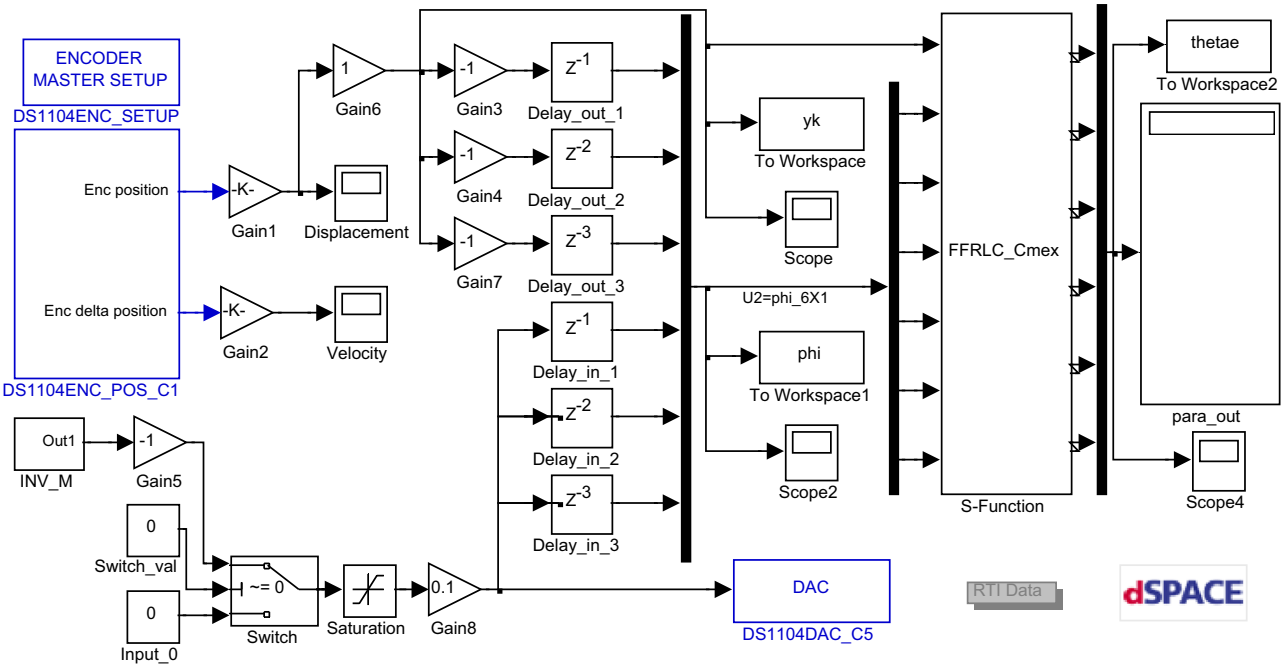

Fig. 26. The experimental block diagram of the FFRLS algorithm.

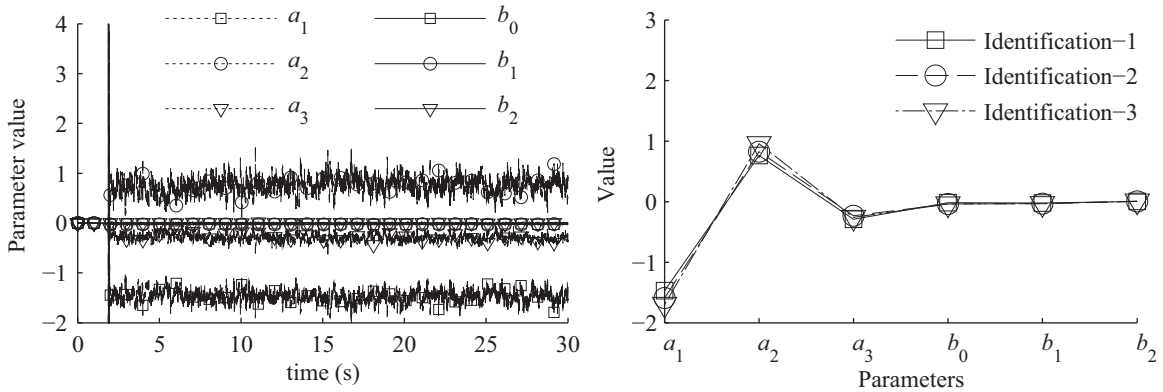

(a) Updating of the parameters in identification (b) Comparison of the three identifications

Fig. 27. Identification results. (a) Updating of the parameters in identification. (b) Comparison of the three identifications.

dead-zone. The dead-zone depth is similar to the simulation in Section 3, taking a value of 0.5 mm. The input signal is a sine wave with an amplitude of 1 mm and a frequency of 0.1 Hz. The simulation results are plotted in Fig. 19 and 20.

Fig. 19 shows signals in the simulation of the adaptive feedback and feedforward control algorithm. The symbols and the meanings of the signals are described in Section 4.2. The simulation shows that the generalized error $e_1(t) = y_{m1}(t) - y_p(t)$ contains the dead-zone nonlinearity, while the tracking error $e_2(t) = y_{m1}(t) - y_{m2}(t)$ does not contain a dead-zone. The generalized error $e_3(t) = e_1(t) - e_2(t)$ is the information on the dead-zone. The amplitude of $e_3(t)$ is the depth of the dead-zone, and the phase of $e_3(t)$ is the moment the dead-zone takes effect. By minimizing $e_3(t)$ through the adaptive law, an adaptive feedforward signal $u_2(t)$ is generated to compensate for the dead-zone. Fig. 19(d) shows that the control signal $u(t)$ is a sine wave signal combined with a peak ($u_2(t)$) in the opposite direction when the dead-zone takes effect. Therefore, it can implement a rapid crossing through the dead-zone, reducing the time in the dead-zone. The tracking result is shown in Fig. 20.

5. Experiments

Experiments were conducted to verify these two control methods. The ultrasonic linear motor positioning system was constructed. The experimental results of the two control algorithms are presented here.

5.1. Introduction of the experimental setup

The experimental apparatus of the whole experimental setup is depicted in Fig. 21(a). The 3PRR precision parallel mechanism driven by three ultrasonic linear motors is shown in Fig. 21(b). The mechanical part of the ultrasonic linear motor positioning system consists of the base plate, motor stands, a linear slider and the ultrasonic linear motor. The electronic part of the system comprises a linear encoder, limit switches, a motor drive unit, a PC and the DS1104 control card.

The PI U-264 ultrasonic linear motor receives the ultrasonic drive voltage from the PI C-872 motor drive unit. Then, it moves with a specific velocity carrying the Renishaw Tonic linear encoder (resolution 0.05 μm). The encoder can measure the actual

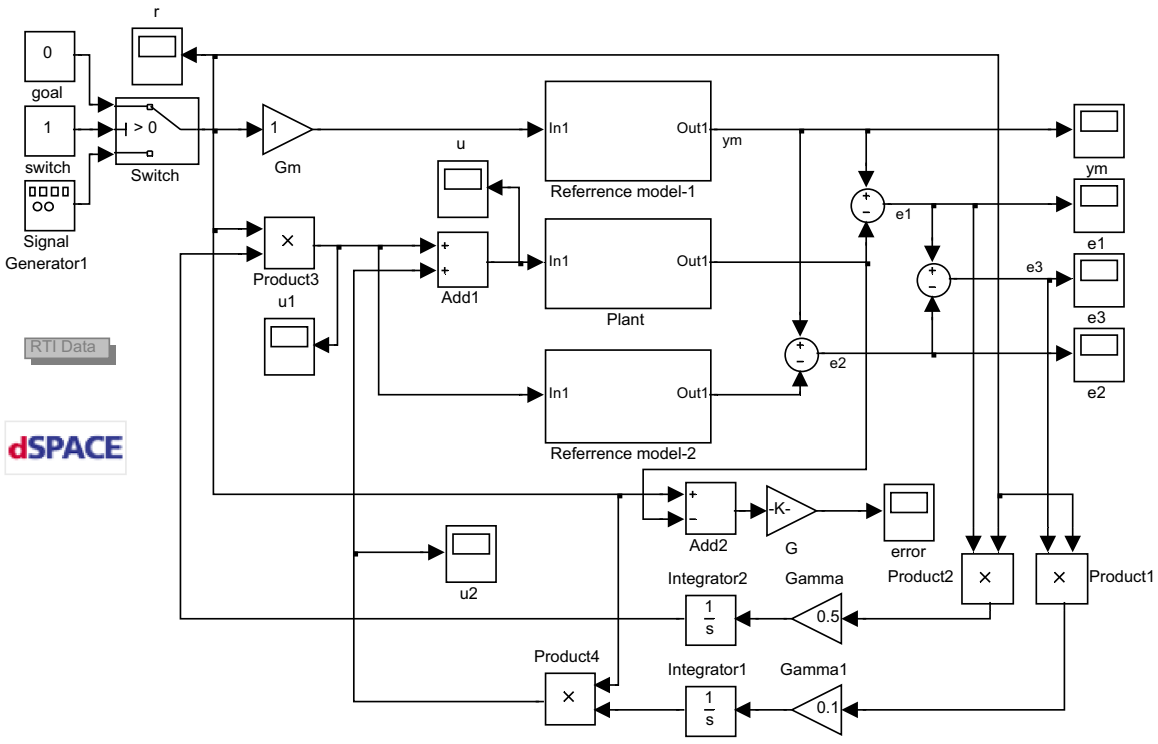

Fig. 28. The experimental block diagram of the adaptive feedback and feedforward control.

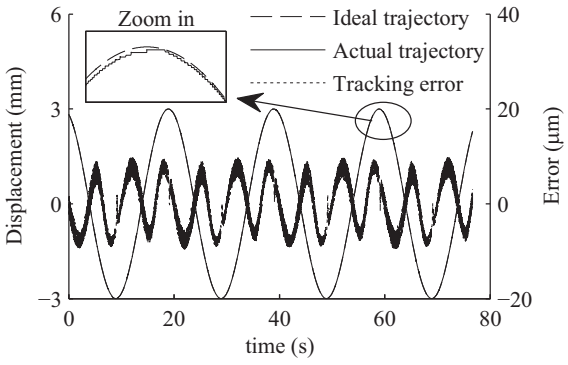

(a) The sine wave tracking result (Sine wave amplitude 3 mm, frequency 0.05 Hz, γ =0.5, γ_1 =0.1)

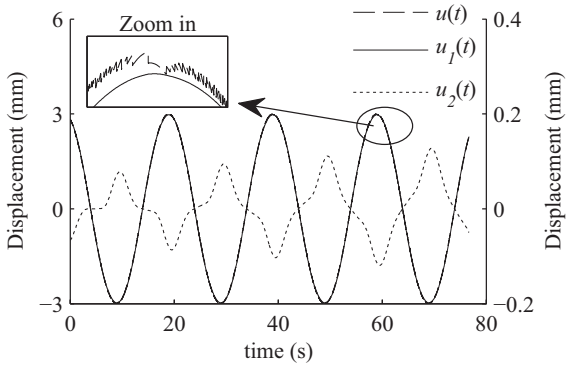

(b) The adaptive control quantity $u(t) = u_1(t) + u_2(t)$

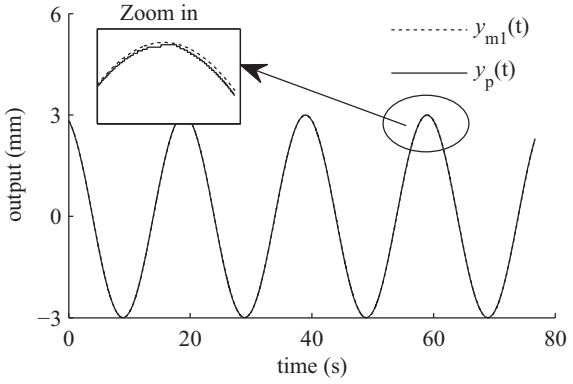

(c) The contrast of $y_{m1}(t)$ and $y_p(t)$

Fig. 29. Experimental results for adaptive control. (a) The sine wave tracking result (Sine wave amplitude 3 mm, frequency 0.05 Hz, $\gamma = 0.5$, $\gamma_1 = 0.1$). (b) The adaptive control quantity $u(t) = u_1(t) + u_2(t)$. (c) The contrast of $y_{m1}(t)$ and $y_p(t)$.

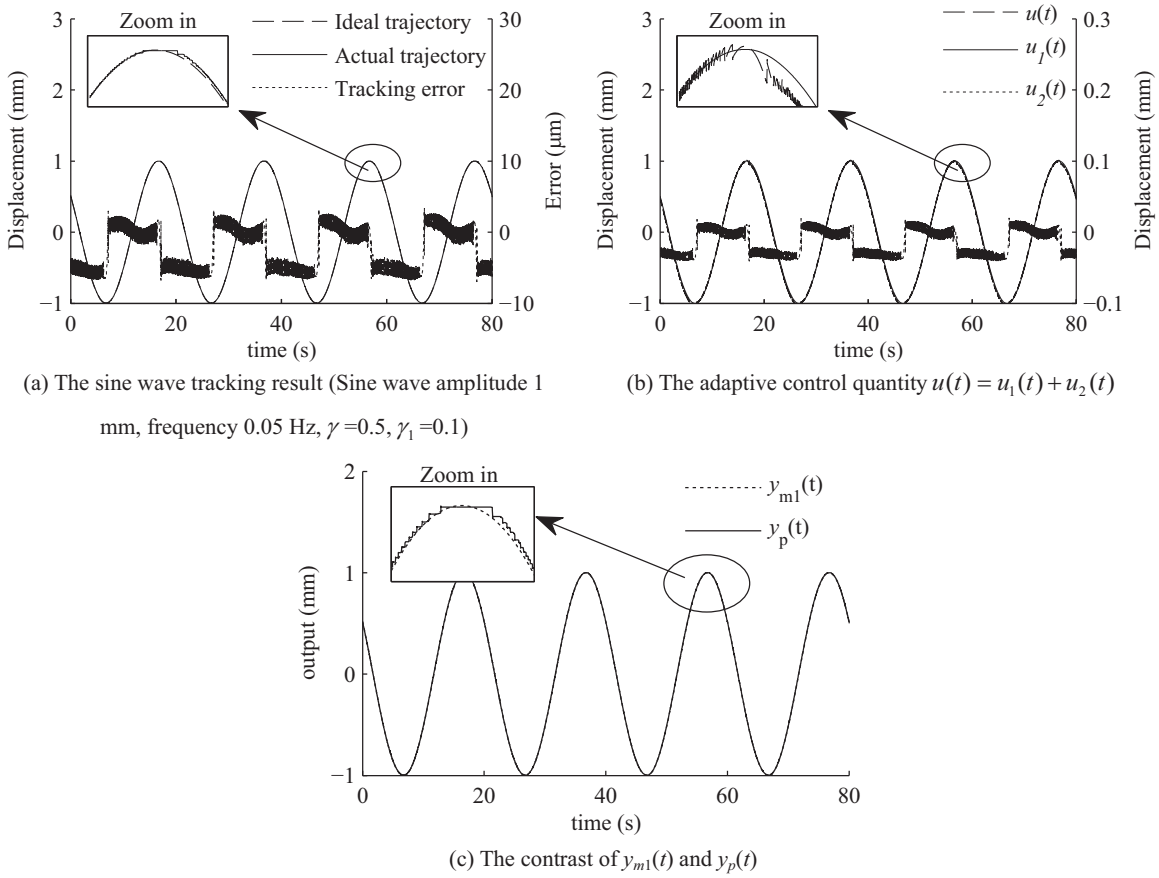

(a) The sine wave tracking result (Sine wave amplitude 1 mm, frequency 0.05 Hz, γ =0.5, γ_1 =0.1)

(b) The adaptive control quantity $u(t) = u_1(t) + u_2(t)$

(c) The contrast of $y_{m1}(t)$ and $y_p(t)$

Fig. 30. Experimental results for adaptive control. (a) The sine wave tracking result (Sine wave amplitude 1 mm, frequency 0.05 Hz, $\gamma = 0.5$, $\gamma_1 = 0.1$). (b) The adaptive control quantity $u(t) = u_1(t) + u_2(t)$. (c) The contrast of $y_{m1}(t)$ and $y_p(t)$.

Table 1
Comparison of the experiment results.

	PID[28]	Feedforward+PID	Adaptive feedback+feedforward
Sine amplitude (μm)	1000.0000	3000.0000	1000.0000
Average error (μm)	16.4906	0.3623	3.2733
Maximum error (μm)	19.6731	5.5305	6.9338
Relative error (%)	1.9673	0.1844	0.6934

displacement and velocity as feedback. The measured signals are sent to the incremental encoder interface of the DS1104 semi-physical simulation card from DSPACE German (sample time 100 μs). The DS1104 receives the displacement signal and sends it to the software interface in SIMULINK/MATLAB and the Control Desk software, programmed using the C language. The control command value is calculated through the specific algorithm, and the command value will be converted to an analog voltage and sent through the DAC interface (16 bits, -10 V_{DC} $\sim +10$ V_{DC}) of DS1104 to the motor drive unit. The motor drive will amplify and convert the DC reference signal to the high-frequency (160 kHz), high-amplitude (up to 200 V) AC drive voltage to the PZT inside the motor case. Thus, the motor adjusts the displacement and velocity in real time. The Omron photoelectric switches are used as the limit switch. The flowchart of positioning control experiments is shown in Fig. 22.

5.2. Constant feedforward with integral separation PID

The control block diagram of this algorithm has been built in SIMULINK/MATLAB and the Control Desk software, as shown in Fig. 23. After tuning, the parameters are selected as $K_p = 25$, $1/T_i = 80$, $T_d = 0.001$, $e_{threshold} = 2.00$ mm, $V_{compensate} = -1.2$ V. The sine wave amplitude is specified as 5.00 mm or 3.00 mm, and its frequency is 2 rad/s. The sine wave tracking results are plotted in Fig. 24 and 25.

Fig. 24(a) shows that the average value of the sine wave tracking error reduces to 0.33 μm, and the average error is shown in Fig. 25(a) to be 0.36 μm after compensation. The peak of the error is less than 6.00 μm in most cases. Compared with the results of Fig. 5, the maximal tracking error is 19.00 μm without compensation. A good effect is obtained after compensation. However, the peak value of the error in Fig. 24(a) is much larger than the others near 10 s. This result demonstrates that this constant value compensator is not very good for the time-varying system. It is suitable for the system with relatively stable parameters and a known dead-zone depth.

5.3. Adaptive feedback and feedforward

To achieve a good control effect, it is necessary to identify the system on line before the positioning experiments because the system is slowly time varying. The system identification uses the FFRLS method. The experimental identification block diagram is shown in Fig. 26. The identification signal is an inverse M sequence.

Fig. 27 shows that the parameters have a fast convergence rate. It requires approximately 2 s for the parameters to converge to a

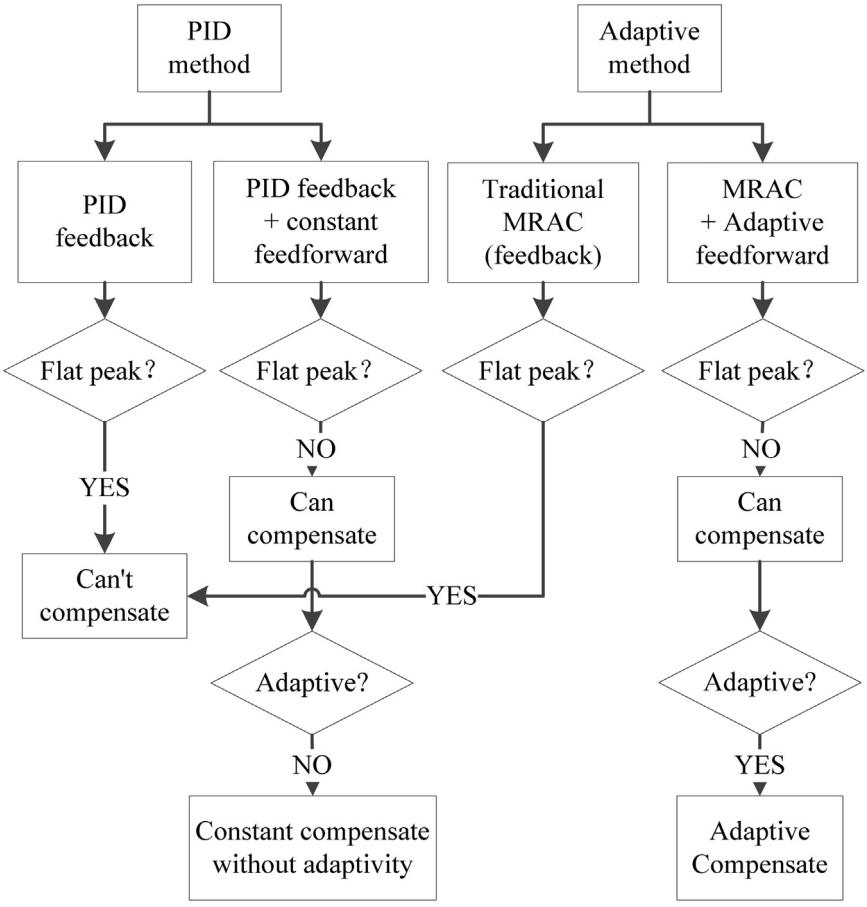

Fig. 31. Comparison of the compensation effects of different algorithms.

constant value when adding the observation noise. To weaken the effect of the observation noise, each parameter is selected as its average value in one of the identification processes. The identification repeats 3 times, and the average value is used to determine the system parameters. The result shows that the FFRLS method has good repeatability. The three identifications are almost the same. After obtaining average values of the six parameters, the system model parameters are $a_1=-1.5848$, $a_2=0.8483$, $a_3=-0.2635$, $b_0=-0.0318$, $b_1=-0.0326$, $b_2=0.0043$.

Eq. (15) is used for reference model 1 and reference model 2. The experimental block diagram is built in SIMULINK/MATLAB and the Control Desk software as shown in Fig. 28.

This algorithm is designed to suit the application of the 3PRR positioning system as the object stage of the SEM. The frequency and distance of the end-effector are limited in the SEM chamber. The explanations are as follows:

1) Frequency: In a micro-nano operation system, the SEM is the observer, and the object stage is used to carry the sample. The refresh rate of the SEM is low. It always takes several seconds to refresh the image, so the performance requirement of the object stage is accuracy instead of rapidity. The experimental frequency of 0.05 Hz means the 3PRR positioning system can achieve 0.1π rad/s angular velocity to run the circular trajectory in the workspace, which is much faster than the refresh rate of the SEM, so better control performance will be achieved in the frequency range below 0.05 Hz.
2) Distance: This 3PRR positioning system is designed in a 12.00 mm radius circle workspace, but the high-accuracy area in the workspace is a 5.00 mm radius circle near the origin point. The driving distance is usually not greater than 5.00 mm, so the experiments in this manuscript correspond to the application of the 3PRR positioning system. In addition, the image magnification of the SEM is high. A long-distance motion will carry the sample out of the field of view. In practical use, therefore, the actual driving distance is much smaller.

The experimental results are plotted in Fig. 29 and 30. These curves match very well, so one can only distinguish them via the zoom in plot or the error curves. The output curves of reference model 1 are the basic tracking signals used for the adaptive feedback control. The generalized error $e_1(t)$ is used to generate the adaptive feedback signal $u_1(t)$, and the generalized error $e_2(t)$ is used to generate the adaptive feedforward signal $u_2(t)$. Figs. 29(c) and 30(c) show that the actual output can track the model output. Figs. 29(a) and 30(a) show that combination with the adaptive feedforward control value $u_2(t)$ can reduce the time in the dead-zone, thus compensating for the flat peak of the sine wave trajectory tracking. The experimental adaptive control value $u(t)$ is shown in Figs. 29(b) and 30(b), similar to the simulation result shown in Fig. 19(d). It is a sine wave signal (basic tracking signal $u_1(t)$) combined with a peak (adaptive feedforward control value $u_2(t)$) in the opposite direction when the dead-zone takes effect. Therefore, it can implement a rapid crossing through the dead-zone to minimize the tracking errors. In Fig. 29, the maximal tracking error is less than 10.00 μm, and the average error is 4.74 μm. In Fig. 30, the maximal tracking error is less than 7.00 μm, and the average error is 3.27 μm.

The innovation in this study is the combination of the adaptive feedback and feedforward controller. This controller divided the

control quantity into two parts, namely, the adaptive feedback part generating the basic tracking signal $u_1(t)$ and the adaptive feedforward part generating the static friction compensation value $u_2(t)$. The value $u_2(t)$ is the key control quantity for solving the flat peak phenomenon because it is the separated value of the static friction. The amplitude of $u_2(t)$ is the compensated value of the dead-zone, and the phase of $u_2(t)$ is the moment when the dead-zone takes effect. Thus, $u_2(t)$ can compensate adaptively for the dead-zone.

5.4. Comparison of experimental results

For comparison with the tracking errors of these different control algorithms, the sine wave trajectory tracking errors are listed in Table 1. Although the sine amplitudes are different, the relative errors are shown to make them comparable. The experimental results demonstrated that the effects of the investigated two control methods are both better than the PID control. These two control methods minimized the sine wave trajectory tracking errors to values below 10.00 μm, and the relative errors to values below 1%, while the errors of the PID control are almost 20.00 μm [28] and the relative errors almost 2%. Comparison of the first and the second method shows that the second method has lower error and higher sine amplitude, which proves that the second method is much better than the first method. The adaptive feedback and feedforward control are slightly worse than the constant feedforward with the integral separation PID, which is because of the reference model. Noise was introduced in the identification model, causing the parameters not to be very precise, and the model structure was simplified by the frequency response test. Because the structure and parameters of the reference model could not be obtained precisely, errors occurred. Although the adaptive feedback and feedforward control are slightly worse than the constant feedforward with the integral separation PID, they are much better than the PID control. The adaptive feedback and feedforward control shows adaptability to the changes in friction interface and is more suitable for the slow-time-varying system.

Through the simulations and experiments, it can be observed that the feedback control algorithm has difficulty compensating effectively for the dead-zone, but in combination with the feedforward control, the control effect is much better. The constant feedforward compensator is not novel but cited from reference [5]. This control algorithm is applied here for two purposes: one is to illuminate the availability of static friction compensation, and the other is to contrast the control effect between these two feedforward compensators. The innovation of this work is the design of a type of adaptive feedforward compensator. The experimental results show that the constant compensator has good control performance when the static friction is invariable and the dead-zone depth has been measured. However, the static friction is usually time varying and uncertain, so the adaptive compensator is more suitable for the static friction compensation. The compensation effect of these algorithms is summarized and shown in Fig. 31.

6. Conclusions

This paper presents the modeling, identification, simulation and experiments on different algorithms to improve the trajectory tracking accuracy of the 3PRR precision parallel mechanism joint positioning control. The experimental results are compared with different algorithms. The adaptive feedback and feedforward controller adopted is more suitable for the ultrasonic linear motor positioning control. The simulation and experimental results demonstrate that the adopted methods can exert satisfactory trajectory tracking control.

Acknowledgements

This work was supported by the National Natural Science Foundation of China (Grant Nos. U1501247 and 91223201), the Natural Science Foundation of Guangdong Province (Grant No. S2013030013355), the Scientific and Technological Project of Guangzhou (Grant No.2015090330001), and the Science and Technology Planning Project of Guangdong Province (Grant No. 2014B090922001). The authors gratefully acknowledge these support agencies.

References

[1] H.C. Liaw, B. Shirinzadeh, Constrained motion tracking control of piezo-actuated flexure-based four-bar mechanisms for micro/nano manipulation, IEEE Trans. Autom. Sci. Eng. 7 (3) (2010) 699–705.
[2] M. Kim, S. Chung, Friction identification of ball-screw driven servomechanisms through the limit cycle analysis, Mechatronics 16 (2) (2006) 131–140.
[3] S.I. Han, J.M. Lee, Adaptive dynamic surface control with sliding mode control and RWNN for robust positioning of a linear motion stage, Mechatronics 22 (2) (2012) 222–238.
[4] S. Liu, Z. Qiu, J. Mo, et al. Experimental Characterization of Self-Excited Vibration of a 3-RRR Parallel Robot, 7th International Conference, ICIRA 2014. Guangzhou, China, December 17–20, 2014.
[5] E. Castillo-Castañeda, Y. Takeda, Improving path accuracy of a crank-type 6-D of parallel mechanism by stiction compensation, Mech. Mach. Theory 43 (1) (2008) 104–114.
[6] Y. Li, S. Tong, T. Li, Adaptive fuzzy output-feedback control for output constrained nonlinear systems in the presence of input saturation, Fuzzy Sets Syst. 248 (2014) 138–155.
[7] Y. Li, S. Tong, T. Li, Adaptive fuzzy output feedback dynamic surface control of interconnected nonlinear pure-feedback systems, IEEE Trans. Cybern. 45 (1) (2015) 138–149.
[8] Y. Li, S. Tong, T. Li, Composite adaptive fuzzy output feedback control design for uncertain nonlinear strict-feedback systems with input saturation, IEEE Trans. Cybern. 45 (10) (2015) 2299–2308.
[9] M. Wang, Y. Kung, C. Chiang, et al. Permanent Magnet Linear Synchronous Motor Drive Design Based On Sliding-Mode Control and Fuzzy Deadzone Estimation, Systems, Man and Cybernetics, 2009, SMC 2009, IEEE International Conference on. IEEE, 2009, pp. 1027–1032.
[10] C.C. De Wit, H. Olsson, K.J. Astrom, et al., A new model for control of systems with friction, Autom. Control, IEEE Trans. 40 (3) (1995) 419–425.
[11] S. Kim, S.H. Kim, A precision linear actuator using piezoelectrically driven friction force, Mechatronics 11 (8) (2001) 969–985.
[12] C.C. De Wit, P. Lischinsky, Adaptive friction compensation with partially known dynamic friction model, Int. J. Adapt. Control Signal Process. 11 (1) (1997) 65–80.
[13] C.T. Johnson, R.D. Lorenz, Experimental identification of friction and its compensation in precise, position controlled mechanisms, IEEE Trans. Ind. Appl. 28 (6) (1992) 1392–1398.
[14] C. Lin, H. Yau, Y. Tian, Identification and compensation of nonlinear friction characteristics and precision control for a linear motor stage, IEEE/ASME Trans. Mechatron. 18 (4) (2013) 1385–1396.
[15] R. Wai, C. Lin, Y. Peng, Adaptive hybrid control for linear piezoelectric ceramic motor drive using diagonal recurrent cmac network, IEEE Trans. Neural Netw. 15 (6) (2004) 1491–1506.
[16] F. Lin, R. Wai, K. Shyu, et al., Recurrent fuzzy neural network control for piezoelectric ceramic linear ultrasonic motor drive, IEEE Trans. Ultrason., Ferroelectr., Freq. Control 48 (4) (2001) 900–913.
[17] F. Lin, R. Wai, M. Chen, Wavelet neural network control for linear ultrasonic motor drive via adaptive sliding-mode technique, IEEE Trans. Ultrason., Ferroelectr., Freq. Control 50 (6) (2003) 686–698.
[18] L. Márton, B. Lantos, Control of mechanical systems with stribeck friction and backlash, Syst. Control Lett. 58 (2) (2009) 141–147.
[19] P.A. Bliman, Mathematical study of the dahl's friction model, Eur. J. Mech. A/Solids 11 (6) (1992) 835–848.
[20] V. Lampaert, J. Swevers, F. Al-Bender, Modification of the leuven integrated friction model Structure, Autom. Control, IEEE Trans. 47 (4) (2002) 683–687.
[21] M.S. Madi, K, Khayati, P. Bigras, Parameter Estimation for the LuGre Friction Model Using Interval Analysis and Set Inversion, Systems, Man and Cybernetics, 2004 IEEE International Conference on, IEEE, 2004, 1, pp. 428–433.
[22] Y.F. Wang, D.H. Wang, T.Y. Chai, Modeling and control compensation of nonlinear friction using adaptive fuzzy systems, Mech. Syst. Signal Process. 23 (8) (2009) 2445–2457.
[23] W. Zhang, X. Ye, Dead zone compensation control of free-floating space robotic manipulators based on neural network, J. Mech. Eng. 50 (13) (2014) 52–58.
[24] Y. Li, S. Tong, Y. Liu, et al., Adaptive fuzzy robust output feedback control of nonlinear systems with unknown dead zones based on a small-gain approach, IEEE Trans. Fuzzy Syst. 22 (1) (2014) 164–176.

[25] Y. Li, S. Tong, T. Li, et al., Adaptive fuzzy control of uncertain stochastic nonlinear systems with unknown dead zone using small-gain approach, Fuzzy Sets Syst. 235 (2014) 1–24.
[26] Y. Li, S. Tong, T. Li, Observer-based adaptive fuzzy tracking control of MIMO stochastic nonlinear systems with unknown control directions and unknown dead zones, IEEE Trans. Fuzzy Syst. 23 (4) (2015) 1228–1241.
[27] C.J. Lin, M.J. Li, K.R. Liu, Tracking control of an ultrasonic linear motor actuated stage using a sliding-mode controller with friction compensation, Smart Sci. (2016).
[28] J. Mo, Z. Qiu, J. Wei, et al. Experimental Study on Joint Positioning Control of an Ultrasonic Linear Motor Driven Planar Parallel Platform, //7th International Conference, ICIRA 2014. Guangzhou, China: December 17–20, 2014.
[29] C. Zhao, Ultrasonic Motor Technology and Application, Springer Science & Business Media, German, 2011.
[30] V.L. Popov, Contact Mechanics and Friction: Physical Principles and Applications, Springer Science & Business Media, German, 2010.
[31] K.J. åström, B. Wittenmark, Adaptive Control, Courier Corporation, 2013.
[32] P.C. Parks, Liapunov Redesign of Model Reference Adaptive Control Systems, IEEE Trans. Autom. Control 11 (3) (1966) 362–367.